Université de Mons
Faculté Polytechnique – Service de Mécanique Rationnelle, Dynamique et Vibrations
31, Bld Dolez - B-7000 MONS (Belgique)
065/37 42 15 – georges.kouroussis@umons.ac.be

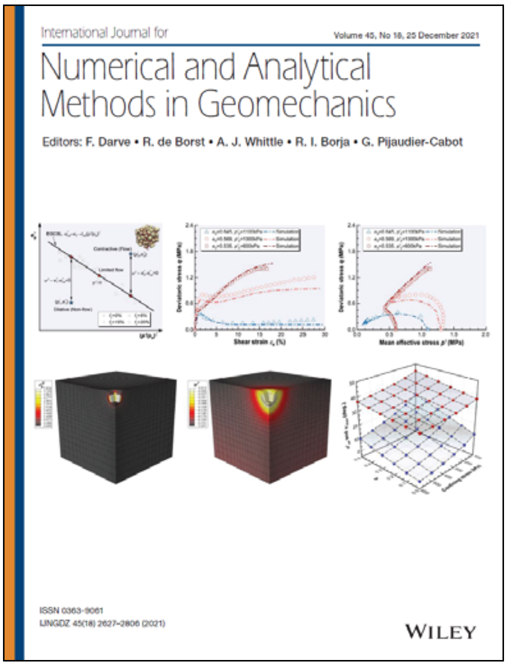

L. Qu, C. Yang, X. Ding, G. Kouroussis, C. Yuan, Vertical vibration of piles with square cross-section, *International Journal for Numerical and Analytical Methods in Geomechanics*, 45 (18), 2629–2653, 2021.

Received: 29 June 2021 | Revised: 13 September 2021 | Accepted: 14 September 2021

DOI: 10.1002/nag.3280

RESEARCH ARTICLE

WILEY

Vertical vibration of piles with square cross-section

Liming Qu[1] | Changwei Yang[1] | Xuanming Ding[2] | Georges Kouroussis[3] | Cheng Yuan[1]

[1] MOE Key Laboratory of High-speed Railway Engineering, College of Civil Engineering, Southwest Jiaotong University, Chengdu, Sichuan Province 610031, China

[2] College of Civil Engineering, Key Laboratory of New Technology for Construction of Cities in Mountain Area, Chongqing University, Chongqing 400045, China

[3] Faculty of Engineering, Department of Theoretical Mechanics, Dynamics and Vibrations, Université de Mons, Mons, Belgium

Correspondence
Changwei Yang, MOE Key Laboratory of High-speed Railway Engineering, College of Civil Engineering, Southwest Jiaotong University, Chengdu, Sichuan Province 610031, China.
Email: 1209732335@qq.com

Funding information
Key Laboratory of New Technology for Construction of Cities in Mountain Area, MOE, Grant/Award Number: LNTCCMA-20210109; China Postdoctoral Science Foundation, Grant/Award Number: 2021M692689; National Natural Science Foundation of China, Grant/Award Number: 52078426; National Key Research and Development Program of China, Grant/Award Number: 2018YFE0207100; 2018 Sichuan province Ten thousand people plan

Abstract
The paper presents an approximate solution to axial dynamic impedance calculation for group of square piles. Firstly, dynamic responses of the single pile-soil system are derived on the basis of Hamilton's energy principle and variation analysis. Then, the effects of square cross section on the pile-soil interaction are examined through the combination of theoretical deduction and numerical simulation. The vertical soil vibration around a square pile is found to be dependent on wave propagation directions in the near field (two times less than the side length of square pile). As the radial distance off pile axis increases, the soil vibration tends to be independent on propagation directions. Through superposition principle, the dynamic impedance of square pile group is calculated. This study could provide a reference to the problems with how the non-circular piles interplay with soil on vibration.

KEYWORDS
interaction factor, soil attenuation, square piles, superposition principle, variation analysis, vertical dynamic impedance

1 | INTRODUCTION

Pile foundations are often subjected to dynamic loads such as vibrating machines, traffic vehicles, earthquakes, wind, and etc.[1–10] The complex dynamic impedance of a pile shaft is defined by the ratio of the external dynamic load acting on the pile head to the induced displacement, which is a critical physical quality estimation of its dynamic performances.[11,12] The real part of the dynamic impedance reflects the corresponding foundation stiffness under various frequencies and the imaginary part indicates the energy dissipation in a mechanical system.

Three types of method considering dynamic vertical pile-soil interaction generally are usually retained: Voigt model,[13] plane strain model,[14–15] and continuum-based model.[16–19] The concept of Voigt model simplifies the effects of soil on the pile as a series of discrete springs and viscous damping. Estimating the pile responses is convenient using Voigt model, but the mechanical coefficients of spring and damping are often empirical and puzzling since their values are independent with the soil properties. The plane strain model ignores the vertical variation of soil stress and thus usually overestimates the dynamic stiffness of piles at the low frequency range. Generally, a continuum model can give a relatively accurate

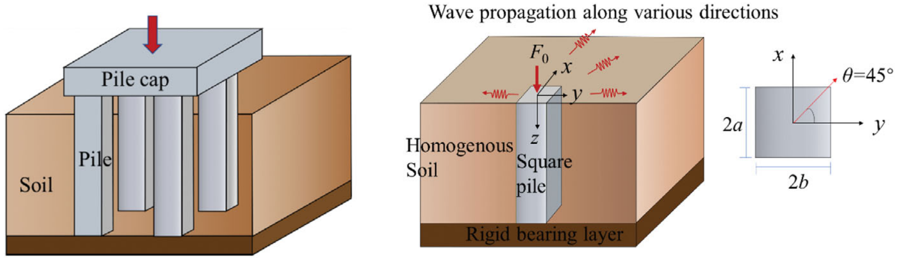

(A) Group of square piles (B) Interaction between soil and a single square pile

FIGURE 1 Illustration of vertically loaded square piles in a homogenous soil and resting on a rigid base

description for the pile-soil interaction by solving analytically the coupling vibration of pile and soil. Many researchers have adopted this type of model to capture the dynamic response of the circular or pipe piles.[20–26]

For the case of pile group, calculating the dynamic impedance of pile group is generally based on the superposition method, which is originally proposed for the static problem and afterwards applied to dynamic problems by Dobry and Gazeta,[27] Gazetas and Makis,[28] Wang et al.,[29] Luan et al.[30] The recent studies[31,32] have proved the efficiency of superposition method using appropriate interaction factors through finite element simulation. According to the superposition method, three steps are required: (1) calculating the dynamic impedance of single piles; (2) estimating the dynamic pile-soil-pile interaction and obtaining the dynamic interaction factor that equal the head displacement ratio between the loaded ("source") pile and the non-loaded ("receiver") pile; (3) employing the superposition principle and establishing the total matrix equation for the dynamic impedance of pile group. However, the traditional analytical solving process becomes considerably complicated when the boundary of soil domain is inclined[33–35] or a non-circular shape of cross section is designed for piles. Practically, concrete piles with square cross section are often used especially when they are prefabricated.[36–41] The dynamic interaction between soil and square piles in a group may not conform to the same rule with that in a circular pile group.

The objective of this study is to examine the effects of square cross section on the vertical dynamic soil-pile interaction. The pile tip condition is considered as end-bearing for sake of simplification. Variation principle is employed to derive the governing equations for a single square pile. The displacement field is formulated by the product of pile displacement and two decay functions of soil.[36,42] The required soil parameters to reach a solution are obtained by an iterative algorithm. According to the results, the effects of square cross section on the complex dynamic impedance and the soil attenuation factor are explored. Further, numerical simulation is carried out to validate and to correct the results from analytical solution to soil attenuation factor. Finally, an approximate method is proposed for the vertical dynamic impedance of square piles in group with the aid of superposition principle.

2 | PROBLEM STATEMENT AND THEORETICAL FRAMEWORK

The problem of interest is the harmonically oscillating square piles installed in a soil layer overlying a rigid bearing layer as illustrated in Figure 1. The pile is routinely considered as a linear elastic shaft with width $2a$, height $2b$, length L, cross section area $A = 4ab$, Mass density ρ_p, and Young's modulus E_p. The soil layer is considered as a homogeneous, isotropic, and linear viscoelastic body with Young's modulus E_s, Poisson's ratio of υ_s, shear modulus $G_s = E_s/[2(1+\upsilon_s]$, density ρ_s, and hysteretic damping ratio β_0. Complex elastic modulus $E_s^* = E_s(1+2\mathrm{i}\beta_0)$, complex shear modulus $G_s^* = E_s^*/[2(1+\upsilon_s)]$, and the Lame's constant $\lambda_s = E_s^*\upsilon_s/[(1+\upsilon_s)(1-2\upsilon_s)]$ are introduced for the soil to simplify the formulation. The pile head is subjected to a harmonic vertical force $F(t) = F_0 e^{\mathrm{i}\omega t}$, where F_0 denotes forcing amplitude, ω represents the excitation frequency, t denotes time and i is the imaginary unit. The pile-soil system is modeled as a continuum and no slippage or separation at soil-pile interfaces is considered.

2.1 | Displacement model for single square pile

Under the vertical excitation, the horizontal displacement u_x and u_y of a pile-soil system is trivial and is thus neglected in this study. The vertical displacement u_z is expressed as:

$$u_z(x,y,z,t) = u_p(z,t)\phi(x)\varphi(y) \tag{1}$$

where $u_p(z,t)$is the time-domain vertical displacement of a pile shaft, $\phi(x)$ and$\varphi(y)$are dimensionless decay functions that are introduced to estimate vibration attenuation in the horizontal direction x and y, respectively. Hence, soil attenuation factor $\psi(x,y)$at the concerning position with coordinate (x, y) is the product of $\phi(x)$and $\varphi(y)$. The inherent boundary conditions for $\phi(x)$ and $\varphi(y)$ can be written as:

$$\phi(x) = \begin{cases} 1, -a \le x \le a \\ 0, x \to \pm\infty \end{cases} \tag{2a}$$

$$\varphi(y) = \begin{cases} 1, -b \le y \le b \\ 0, y \to \pm\infty \end{cases} \tag{2b}$$

Assume that the load at pile head is denoted by P. Then the dynamic impedance k_d of single pile can be expressed by:

$$k_d = \frac{F}{u_z} \tag{2c}$$

For the sake of clarity, detailed deduction for k_d is put on Section 3 on the basis of Hamilton's energy principle and variation analysis.

2.2 | Describing pile-to-pile interaction

The interaction between the loaded pile and receiver pile can be expressed in the form of displacement as following:

$$\alpha = \psi(x,y)\xi \tag{3}$$

where $\alpha$is the interaction factor that quantitively describe the pile-to-pile interaction; $\psi(x,y)$represents the soil attenuation factor;ξ denotes the diffraction factor which accounts for the wave diffraction effects in the presence of receiver piles,[13,34] and its value for the case of end-bearing piles in horizontal ground can be calculated through:

$$\xi = \frac{k_s}{2(k_s - \rho_p A\omega^2)}\left[1 - \frac{2L\sqrt{\frac{k_s-\rho_p A\omega^2}{E_p A}}}{\sinh(2L\sqrt{\frac{k_s-\rho_p A\omega^2}{E_p A}})}\right] \tag{4}$$

where k_s represents the dynamic soil resistance acting on pile shaft.

2.3 | Solving the dynamic impedance of pile group

Here we consider the case that the pile cap is right above the ground level and thus no direct stress transfer occurs between the pile cap and soil. With the aid of superposition method, the governing matrix equation for the M identical square piles that are connected through a no-mass rigid cap is written as:

$$\begin{bmatrix} 0 & 1 & 1 & \dots & 1 \\ -1 & \beta_{11} & \beta_{12} & \dots & \beta_{1M} \\ -1 & \beta_{21} & 1 & \dots & \beta_{2M} \\ \dots & \dots & \dots & \dots & \dots \\ -1 & \beta_{M1} & \beta_{M2} & \dots & \beta_{MM} \end{bmatrix} \begin{Bmatrix} u_G \frac{E_p A_p}{L} \\ P_1 \\ P_2 \\ \dots \\ P_M \end{Bmatrix} = \begin{Bmatrix} F_G \\ 0 \\ 0 \\ \dots \\ 0 \end{Bmatrix} \tag{5}$$

where u_G denotes the vertical displacement of the cap; F_i denote the load acting on the head of pile i and F_G is the external force acting on the cap; the coefficient β_{ij} can be calculated as following:

$$\beta_{ij} = \frac{E_p A_p}{k_d^j L}\alpha_{ij} \tag{6}$$

where k_d^j denotes the dynamic impedance of pile j; α_{ij} equals the vertical displacement of the unloaded pile i when the loaded pile j undergoes a unit displacement. The interaction factor α_{ij} should equals α_{ji} for identical circular piles. However, for square piles, the rationality of that equation $\alpha_{ij} = \alpha_{ji}$ remains further study, which will be done in Section 5.

Once Equation (6) is solved, the dynamic impedance for a group of square piles can be expressed by:

$$k_G = F_G / u_G \tag{7}$$

3 ANALYTICAL SOLUTIONS TO VIBRATION RESPONSES OF SINGLE SQUARE PILES

3.1 Energy formations and Hamilton's principle

From the displacement model for individual square piles in Section 2.1, the non-zero stress and strain components in soil field can be written as:

$$\begin{bmatrix} \varepsilon_{zz} \\ \gamma_{xz} \\ \gamma_{yz} \\ \sigma_{zz} \\ \tau_{xz} \\ \tau_{yz} \end{bmatrix} = \begin{bmatrix} -\partial u_z/\partial z \\ -\left(\partial u_z/\partial x\right)/2 \\ -\left(\partial u_z/\partial y\right)/2 \\ -\left(\lambda_s + 2G_s^*\right)\partial u_z/\partial z \\ -2G_s^*\left(\partial u_z/\partial x\right) \\ -2G_s^*\left(\partial u_z/\partial y\right) \end{bmatrix} \tag{8}$$

In a soil-pile system undergoing vertical wave excitation, the involved total energy includes the kinetic energy (T), the potential energy (U) and the work (W) defined by external forces. These energy components are given by the following:

$$T = \int_0^L \frac{1}{2}\rho_p A \left(\frac{\partial u_p}{\partial t}\right)^2 dz + \iiint_{\Omega_0} \frac{1}{2}\rho_s \phi^2 \varphi^2 \left(\frac{\partial u_p}{\partial t}\right)^2 d\Omega \tag{9}$$

$$\mathrm{U} = \int_0^L \frac{1}{2}E_p A \left(\frac{\partial u_p}{\partial z}\right)^2 dz + \frac{1}{2}\iiint_{\Omega_0} \left(\sigma_{zz}\varepsilon_{zz} + \tau_{xz}\gamma_{xz} + \tau_{yz}\gamma_{yz}\right) d\Omega \tag{10}$$

$$W = F u_{p,z=0} \tag{11}$$

where the first terms in Equation (9) and Equation (10) represent the energy stored in the pile, and the second term represents the energy in the soil domain Ω_0.

According to Hamilton's principle, the energy function $\mathfrak{R}$ from initial time t_1 to final time t_2 of a soil-pile system gets the minimal value at the equilibrium state, which yields:

$$\delta\mathfrak{R} = \int_{t_1}^{t_2} (\delta T - \delta U + \delta W) dt = 0 \tag{12}$$

where δ is the variational operator.

Note that the vertical vibration response of a square pile is symmetric with respect to both x axis and y axis. Therefore, Equation (12) can be expressed as:

$$\begin{aligned}
\delta\mathfrak{R} &= \frac{1}{2}\rho_{\mathrm{p}}A\int_{t_1}^{t_2}\int_0^L \delta\left(\frac{\partial u_{\mathrm{p}}}{\partial t}\right)^2 dzdt + 2\rho_{\mathrm{s}}\int_{t_1}^{t_2}\int_0^a\int_b^{+\infty}\delta\left\{\phi^2\varphi^2\left(\frac{\partial u_{\mathrm{p}}}{\partial t}\right)^2\right\}dxdydt\\
&+2\rho_{\mathrm{s}}\int_{t_1}^{t_2}\int_a^{+\infty}\int_b^{+\infty}\delta\left\{\phi^2\varphi^2\left(\frac{\partial u_{\mathrm{p}}}{\partial t}\right)^2\right\}dxdydt + 2\rho_{\mathrm{s}}\int_{t_1}^{t_2}\int_a^{\infty}\int_0^{b}\delta\left\{\phi^2\varphi^2\left(\frac{\partial u_{\mathrm{p}}}{\partial t}\right)^2\right\}dxdydt\\
&-\frac{1}{2}E_{\mathrm{p}}A\int_{t_1}^{t_2}\int_0^L\delta\left(\frac{\partial u_{\mathrm{p}}}{\partial z}\right)^2 dzdt - 2\int_{t_1}^{t_2}\int_0^L\int_a^\infty\int_b^\infty\delta\left[(\lambda_{\mathrm{s}}+2G_{\mathrm{s}}^*)\left(\frac{du}{dz}\right)^2\phi^2(x)\varphi^2(y) + G_{\mathrm{s}}^*u^2\left(\frac{d\phi}{dx}\right)^2\varphi^2 + G_{\mathrm{s}}^*u^2\left(\frac{d\varphi}{dy}\right)^2\phi^2(x)\right]dxdydzdt\\
&-2\int_{t_1}^{t_2}\int_0^L\int_a^\infty\int_0^b\delta\left[(\lambda_{\mathrm{s}}+2G_{\mathrm{s}}^*)\left(\frac{du}{dz}\right)^2\phi^2(x)\varphi^2(y) + G_{\mathrm{s}}^*u^2\left(\frac{d\phi}{dx}\right)^2\varphi_{\mathrm{y}}^2 + G_{\mathrm{s}}^*u^2\left(\frac{d\varphi}{dy}\right)^2\phi^2(x)\right]dxdydzdt\\
&-2\int_{t_1}^{t_2}\int_0^L\int_0^a\int_b^\infty\delta\left[(\lambda_{\mathrm{s}}+2G_{\mathrm{s}}^*)\left(\frac{du}{dz}\right)^2\phi^2(x)\varphi^2(y) + G_{\mathrm{s}}^*u^2\left(\frac{d\phi}{dx}\right)^2\varphi_{\mathrm{y}}^2 + G_{\mathrm{s}}^*u^2\left(\frac{d\varphi}{dy}\right)^2\phi^2(x)\right]dxdydzdt - \int_{t_1}^{t_2}F\delta u_{\mathrm{p}}\,|_{z=0}\,dt\\
&= 0
\end{aligned} \tag{13}$$

3.2 | Governing equations of pile vibration

Collecting the coefficients of $\delta u_{\mathrm{p}}$from the variational analysis in Equation (13), the following equation can be obtained:

$$\begin{aligned}
&\rho_{\mathrm{p}}A\int_0^L\delta u_{\mathrm{p}}\frac{\partial u_{\mathrm{p}}}{\partial t}\Big|_{t_1}^{t_2}dz - \rho_{\mathrm{p}}A\int_0^L\int_{t_1}^{t_2}\frac{\partial^2 u_{\mathrm{p}}}{\partial t^2}\delta u_{\mathrm{p}}dtdz - E_{\mathrm{p}}A\int_{t_1}^{t_2}\frac{\partial u_{\mathrm{p}}}{\partial z}\delta u_{\mathrm{p}}\Big|_0^L dt + E_{\mathrm{p}}A\int_0^L\int_{t_1}^{t_2}\delta u_{\mathrm{p}}\frac{\partial^2 u_{\mathrm{p}}}{\partial z^2}dzdt\\
&+4\rho_{\mathrm{s}}\left[\int_a^\infty\int_b^\infty\phi^2(x)\varphi^2(y)dxdy + \int_a^\infty\int_0^b\phi^2(x)\varphi^2(y)dxdy + \int_0^a\int_b^\infty\phi^2(x)\varphi^2(y)dxdy\right]\int_0^L\int_{t_1}^{t_2}\frac{\partial u_{\mathrm{p}}}{\partial t}\delta u_{\mathrm{p}}\Big|_{t_1}^{t_2}dzdt\\
&-4(\lambda_{\mathrm{s}}+2G_{\mathrm{s}}^*)\left[\int_a^\infty\int_b^\infty\phi^2(x)\varphi^2(y)dxdy + \int_a^\infty\int_0^b\phi^2(x)\varphi^2(y)dxdy + \int_0^a\int_b^\infty\phi^2(x)\varphi^2(y)dxdy\right]\int_{t_1}^{t_2}\frac{\partial u_{\mathrm{p}}}{\partial z}\delta u_{\mathrm{p}}\Big|_0^L dt\\
&-4\rho_s\left[\int_a^\infty\int_b^\infty\phi^2(x)\varphi^2(y)dxdy + \int_a^\infty\int_0^b\phi^2(x)\varphi^2(y)dxdy + \int_0^a\int_b^\infty\phi^2(x)\varphi^2(y)dxdy\right]\int_0^L\int_{t_1}^{t_2}\frac{\partial^2 u_{\mathrm{p}}}{\partial t^2}\delta u_{\mathrm{p}}dtdz\\
&+4(\lambda_{\mathrm{s}}+2G_{\mathrm{s}}^*)\left[\int_a^\infty\int_b^\infty\phi^2(x)\varphi^2(y)dxdy + \int_a^\infty\int_0^b\phi^2(x)\varphi^2(y)dxdy + \int_0^a\int_b^\infty\phi^2(x)\varphi^2(y)dxdy\right]\int_0^L\int_{t_1}^{t_2}\frac{\partial^2 u_{\mathrm{p}}}{\partial z^2}\delta u_{\mathrm{p}}dzdt\\
&-4G_{\mathrm{s}}^*\left[\int_a^\infty\int_b^\infty\left(\frac{d\phi_{\mathrm{x}}}{dx}\right)^2\varphi_{\mathrm{y}}^2dxdy + \int_a^\infty\int_0^b\left(\frac{d\phi_{\mathrm{x}}}{dx}\right)^2\varphi_{\mathrm{y}}^2dxdy + \int_0^a\int_b^\infty\left(\frac{d\phi_{\mathrm{x}}}{dx}\right)^2\varphi_{\mathrm{y}}^2dxdy\right]\int_0^L\int_{t_1}^{t_2}u_{\mathrm{p}}\delta u_{\mathrm{p}}dzdt\\
&-4G_{\mathrm{s}}^*\left[\int_a^\infty\int_b^\infty\left(\frac{d\varphi_{\mathrm{y}}}{dy}\right)^2\phi^2(x)dxdy + \int_a^\infty\int_0^b\left(\frac{d\varphi_{\mathrm{y}}}{dy}\right)^2\phi^2(x)dxdy + \int_0^a\int_b^\infty\left(\frac{d\varphi_{\mathrm{y}}}{dy}\right)^2\phi^2(x)dxdy+\right]\int_0^L\int_{t_1}^{t_2}u_{\mathrm{p}}\delta u_{\mathrm{p}}dzdt\\
&-\int_{t_1}^{t_2}F\delta u_{\mathrm{p}}\,|_{z=0}\,dt\\
&=0
\end{aligned} \tag{14}$$

Applying Hamilton's principle, and introducing the harmonic vibration condition, the governing equation of the pile displacement u_{p} can be written as:

$$\begin{aligned}
&\left\{E_{\mathrm{p}}A + 4(\lambda_{\mathrm{s}}+2G_{\mathrm{s}}^*)\left[\int_a^\infty\int_b^\infty\phi^2(x)\varphi^2(y)dxdy + \int_a^\infty\int_0^b\phi^2(x)\varphi^2(y)dxdy + \int_0^a\int_b^\infty\phi^2(x)\varphi^2(y)dxdy\right]\right\}\frac{\partial^2 u_{\mathrm{p}}}{\partial z^2}\\
&+\left\{\omega^2\rho_{\mathrm{p}}A + 4\rho_{\mathrm{s}}\omega^2\left[\int_a^\infty\int_b^\infty\phi^2(x)\varphi^2(y)dxdy + \int_a^\infty\int_0^b\phi^2(x)\varphi^2(y)dxdy + \int_0^a\int_b^\infty\phi^2(x)\varphi^2(y)dxdy\right]\right\}u_{\mathrm{p}}\\
&-4G_{\mathrm{s}}^*\left[\int_a^\infty\int_b^\infty\left(\frac{d\phi_{\mathrm{x}}}{dx}\right)^2\varphi_{\mathrm{y}}^2dxdy + \int_a^\infty\int_0^b\left(\frac{d\phi_{\mathrm{x}}}{dx}\right)^2\varphi_{\mathrm{y}}^2dxdy + \int_0^a\int_b^\infty\left(\frac{d\phi_{\mathrm{x}}}{dx}\right)^2\varphi_{\mathrm{y}}^2dxdy + \int_a^\infty\int_b^\infty\left(\frac{d\varphi_{\mathrm{y}}}{dy}\right)^2\phi^2(x)dxdy + \int_a^\infty\int_0^b\left(\frac{d\varphi_{\mathrm{y}}}{dy}\right)^2\phi^2(x)dxdy + \int_0^a\int_b^\infty\left(\frac{d\varphi_{\mathrm{y}}}{dy}\right)^2\phi^2(x)dxdy\right]u_{\mathrm{p}}\\
&=0
\end{aligned} \tag{15}$$

with boundary conditions:

$$
\begin{aligned}
&\rho_{\mathrm{p}} A \int_0^L \frac{\partial u_{\mathrm{p}}}{\partial t} \Big|_{t_1}^{t_2} dz + 4\rho_{\mathrm{s}} \left[\int_a^\infty \int_b^\infty \phi^2(x)\varphi^2(y)dxdy + \int_a^\infty \int_0^b \phi^2(x)\varphi^2(y)dxdy + \int_0^a \int_b^\infty \phi^2(x)\varphi^2(y)dxdy \right] \int_0^L \frac{\partial u_{\mathrm{p}}}{\partial t} \Big|_{t_1}^{t_2} dz - E_{\mathrm{p}} A \frac{\partial u_{\mathrm{p}}}{\partial z} \Big|_0^L \\
&-4\left(\lambda_{\mathrm{s}} + 2G_{\mathrm{s}}^*\right) \left[\int_a^\infty \int_b^\infty \phi^2(x)\varphi^2(y)dxdy + \int_a^\infty \int_0^b \phi^2(x)\varphi^2(y)dxdy + \int_0^a \int_b^\infty \phi^2(x)\varphi^2(y)dxdy \right] \frac{\partial u_{\mathrm{p}}}{\partial z} \Big|_0^L - F_0 \big|_{z=0} = 0
\end{aligned}
\tag{16}
$$

and

$$
u_{\mathrm{p}} \big|_{z=L} = 0 \tag{17}
$$

Equation (15) can be changed as:

$$
\left[E_{\mathrm{p}} A + \left(\lambda_{\mathrm{s}} + 2G_{\mathrm{s}}^*\right) \xi\right] \frac{d^2 u_{\mathrm{p}}}{dz^2} + \rho_{\mathrm{p}} A \omega^2 u_{\mathrm{p}} - \left(k - \omega^2 \rho_{\mathrm{s}} \xi\right) u_{\mathrm{p}} = 0 \tag{18}
$$

where

$$
k = 4G_{\mathrm{s}}^* \left[\left(p_{\mathrm{x2}} q_{\mathrm{y2}} + p_{\mathrm{x2}} q_{\mathrm{y1}} + p_{\mathrm{x1}} q_{\mathrm{y2}}\right) + \left(p_{\mathrm{y2}} q_{\mathrm{x2}} + p_{\mathrm{y2}} q_{\mathrm{x1}} + p_{\mathrm{y1}} q_{\mathrm{x2}}\right)\right] \tag{19a}
$$

$$
\xi = 4\left(q_{\mathrm{x2}} q_{\mathrm{y2}} + q_{\mathrm{x2}} q_{\mathrm{y1}} + q_{\mathrm{x1}} q_{\mathrm{y2}}\right) \tag{19b}
$$

$$
p_{\mathrm{x1}} = \int_0^a \left(\frac{d\phi}{dx}\right)^2 dx \tag{19c}
$$

$$
p_{\mathrm{x2}} = \int_a^\infty \left(\frac{d\phi}{dx}\right)^2 dx \tag{19d}
$$

$$
p_{\mathrm{y1}} = \int_0^b \left(\frac{d\varphi}{dy}\right)^2 dy \tag{19e}
$$

$$
p_{\mathrm{y2}} = \int_b^\infty \left(\frac{d\varphi}{dy}\right)^2 dy \tag{19f}
$$

$$
q_{\mathrm{x1}} = \int_0^a \phi^2 dx \tag{19g}
$$

$$
q_{\mathrm{x2}} = \int_a^\infty \phi^2 dx \tag{19h}
$$

$$
q_{\mathrm{y1}} = \int_0^b \varphi^2 dy \tag{19n}
$$

$$
q_{\mathrm{y2}} = \int_b^\infty \varphi^2 dy \tag{19m}
$$

In Equation (18), the first term on the left represents the axial compression from the pile and soil; the second term on the left reflects the axial inertia of vibration pile shaft; and the third term represents the dynamic soil resistance acting on the pile perimeter. The general solution for u_{p} can be given by:

$$u_{\mathrm{p}} = c_1 e^{\chi z} + c_2 e^{-\chi z} \tag{20}$$

where

$$\chi = \sqrt{\frac{k - \left(\rho_{\mathrm{p}} A + \rho_{\mathrm{s}} \xi\right) \omega^2}{\left(\lambda_{\mathrm{s}} + 2G_{\mathrm{s}}^*\right) \xi + E_{\mathrm{p}} A}} \tag{21}$$

and c_1, c_2 are the integration constants which are determined by the boundary conditions in Equation (16) and Equation (17). Considering the variation definition, the first and second terms on the left side of Equation (16) equal zero. Consequently, the boundary conditions of Equation (16) and Equation (17) can be simplified as:

$$\left\{ E_{\mathrm{p}} A \frac{\partial u_{\mathrm{p}}}{\partial z} + \left(\lambda_{\mathrm{s}} + 2G_{\mathrm{s}}^*\right) q_{\mathrm{x}} q_{\mathrm{y}} \frac{\partial u_{\mathrm{p}}}{\partial z} - F_0 \right\} |_{z=0} = 0 \tag{22}$$

$$u_{\mathrm{p}} = \frac{F_0}{\sqrt{\left[E_{\mathrm{p}} A + \left(\lambda_{\mathrm{s}} + 2G_{\mathrm{s}}^*\right) \xi\right] \left[k - \left(\rho_{\mathrm{p}} A + \rho_{\mathrm{s}} \xi\right) \omega^2\right]}} \frac{e^{-\chi(L-z)} - e^{\chi(L-z)}}{e^{\chi L} + e^{-\chi L}} \tag{23}$$

Hence the dynamic impedance of pile at head can be written as:

$$k_{\mathrm{d}} = \frac{F_0}{u_{\mathrm{p}}} = \sqrt{\left[E_{\mathrm{p}} A + \left(\lambda_{\mathrm{s}} + 2G_{\mathrm{s}}^*\right) \xi\right] \left[k - \left(\rho_{\mathrm{p}} A + \rho_{\mathrm{s}} \xi\right) \omega^2\right]} \frac{e^{2\chi L} + 1}{1 - e^{2\chi L}} \tag{24}$$

3.3 | Governing equations of soil vibration

In Section 3.1, the vertical displacement of soil on vibration is expressed in the form of the product of pile displacement and the corresponding soil attenuation factor. The latter factor is determined by the decay functions $\phi(x)$ and $\varphi(y)$. Considering Hamilton's principle and collecting the coefficients of $\delta\phi(x)$, the governing equation of $\phi(x)$can be obtained as follows:

$$\frac{d^2 \phi_{\mathrm{x}}}{dx^2} - \left(\frac{\gamma_{\mathrm{x}}}{\gamma_{\mathrm{p}}}\right)^2 \phi = 0 \tag{25}$$

where γ_{x} is introduced as a parameter to characterize the decay function of soil displacement, which can be written as:

$$\left(\frac{\gamma_{\mathrm{x}}}{\gamma_{\mathrm{p}}}\right)^2 = \left(\frac{\lambda_{\mathrm{s}} + 2G_{\mathrm{s}}^*}{G_{\mathrm{s}}^*}\right) \frac{n}{m} + \frac{p_{\mathrm{y1}} + p_{\mathrm{y2}}}{q_{\mathrm{y1}} + q_{\mathrm{y2}}} - \frac{\rho_{\mathrm{s}} \omega^2}{G_{\mathrm{s}}^*} \tag{26}$$

in which

$$m = \int_0^L {u_{\mathrm{p}}}^2 dz = \frac{F_0^2}{\left[E_{\mathrm{p}} A + \left(\lambda_{\mathrm{s}} + 2G_{\mathrm{s}}^*\right) \xi\right] \left[k - \left(\rho_{\mathrm{p}} A + \rho_{\mathrm{s}} \xi\right) \omega^2\right] \left(e^{2\chi L} + e^{-2\chi L}\right)} \left[\frac{\sinh(2L\chi)}{\chi} - 2L\right] \tag{27}$$

$$n = \int_0^L \left(\frac{du}{dz}\right)^2 dz = \frac{\chi^2 F_0^2}{\left[E_{\mathrm{p}} A + \left(\lambda_{\mathrm{s}} + 2G_{\mathrm{s}}^*\right) \xi\right] \left[k - \left(\rho_{\mathrm{p}} A + \rho_{\mathrm{s}} \xi\right) \omega^2\right] \left(e^{2\chi L} + e^{-2\chi L}\right)} \left[\frac{\sinh(2L\chi)}{\chi} + 2L\right] \tag{28}$$

Also, considering Hamilton's principle and collecting the coefficients of $\delta\varphi(y)$, the governing equation of $\varphi(y)$can be obtained as follows:

$$\frac{d^2 \varphi}{dy^2} - \left(\frac{\gamma_{\mathrm{y}}}{\gamma_{\mathrm{p}}}\right)^2 \varphi = 0 \tag{29}$$

where

$$\left(\frac{\gamma_{\mathrm{y}}}{\gamma_{\mathrm{p}}}\right)^2=\left(\frac{\lambda_{\mathrm{s}}+2G_{\mathrm{s}}^*}{G_{\mathrm{s}}^*}\right)\frac{n}{m}+\frac{p_{\mathrm{x}1}+p_{\mathrm{x}2}}{q_{\mathrm{x}1}+q_{\mathrm{x}2}}-\frac{\rho_{\mathrm{s}}\omega^2}{G_{\mathrm{s}}^*} \tag{30}$$

Given the boundary conditions in Equations (2a) and (2b), the solutions of $\phi(x)$,$\varphi(y)$are written as:

$$\phi(x)=\begin{cases} e^{\left(\frac{\gamma_{\mathrm{x}}}{r_{\mathrm{p}}}(x+a)\right)}, x\le -a \\ 1, -a<x\le a \\ e^{\left(-\frac{\gamma_{\mathrm{x}}}{r_{\mathrm{p}}}(x-a)\right)}, x>a \end{cases} \tag{31a}$$

$$\varphi(y)=\begin{cases} e^{\left(\frac{\gamma_{\mathrm{y}}}{r_{\mathrm{p}}}(y+b)\right)}, y\le -b \\ 1, -b<y\le b \\ e^{\left(-\frac{\gamma_{\mathrm{y}}}{r_{\mathrm{p}}}(y-b)\right)}, y>b \end{cases} \tag{31b}$$

Substituting Equations (31a) and (31b) into Equations (19a-m) yields the following:

$$k=G_{\mathrm{s}}\left(\frac{\gamma_{\mathrm{x}}}{\gamma_{\mathrm{y}}}+\frac{2\gamma_{\mathrm{x}}}{r_{\mathrm{p}}}b+\frac{\gamma_{\mathrm{y}}}{\gamma_{\mathrm{x}}}+\frac{2\gamma_{\mathrm{y}}}{r_{\mathrm{p}}}a\right) \tag{32a}$$

$$\xi=4\left(\frac{r_{\mathrm{p}}}{2\gamma_{\mathrm{x}}}\frac{r_{\mathrm{p}}}{2\gamma_{\mathrm{y}}}+\frac{r_{\mathrm{p}}}{2\gamma_{\mathrm{x}}}b+\frac{r_{\mathrm{p}}}{2\gamma_{\mathrm{y}}}a\right) \tag{32b}$$

$$p_{\mathrm{x}1}=0 \tag{32c}$$

$$p_{\mathrm{x}2}=\frac{\gamma_{\mathrm{x}}}{2r_{\mathrm{p}}} \tag{32d}$$

$$p_{\mathrm{y}1}=0 \tag{32e}$$

$$p_{\mathrm{y}2}=\frac{\gamma_{\mathrm{y}}}{2r_{\mathrm{p}}} \tag{32f}$$

$$q_{\mathrm{x}1}=a \tag{32g}$$

$$q_{\mathrm{x}2}=\frac{r_{\mathrm{p}}}{2\gamma_{\mathrm{x}}} \tag{32h}$$

$$q_{\mathrm{y}1}=b \tag{32n}$$

$$q_{\mathrm{y}2}=\frac{r_{\mathrm{p}}}{2\gamma_{\mathrm{y}}} \tag{32m}$$

Specially, when the cross-section of a pile is square and thus $a=b$, Equations (19a, b), Equations (32a), 32(b) can be simplified as:

$$\gamma_{\mathrm{x}}=\gamma_{\mathrm{y}}=\gamma_{\mathrm{p}}\sqrt{\left(\frac{\lambda_{\mathrm{s}}+2G_{\mathrm{s}}^*}{G_{\mathrm{s}}^*}\right)\frac{n}{m}+\frac{\gamma_{\mathrm{x}}^2}{2a^2\gamma_{\mathrm{x}}+a^2}-\frac{\rho_{\mathrm{s}}\omega^2}{G_{\mathrm{s}}^*}} \tag{33}$$

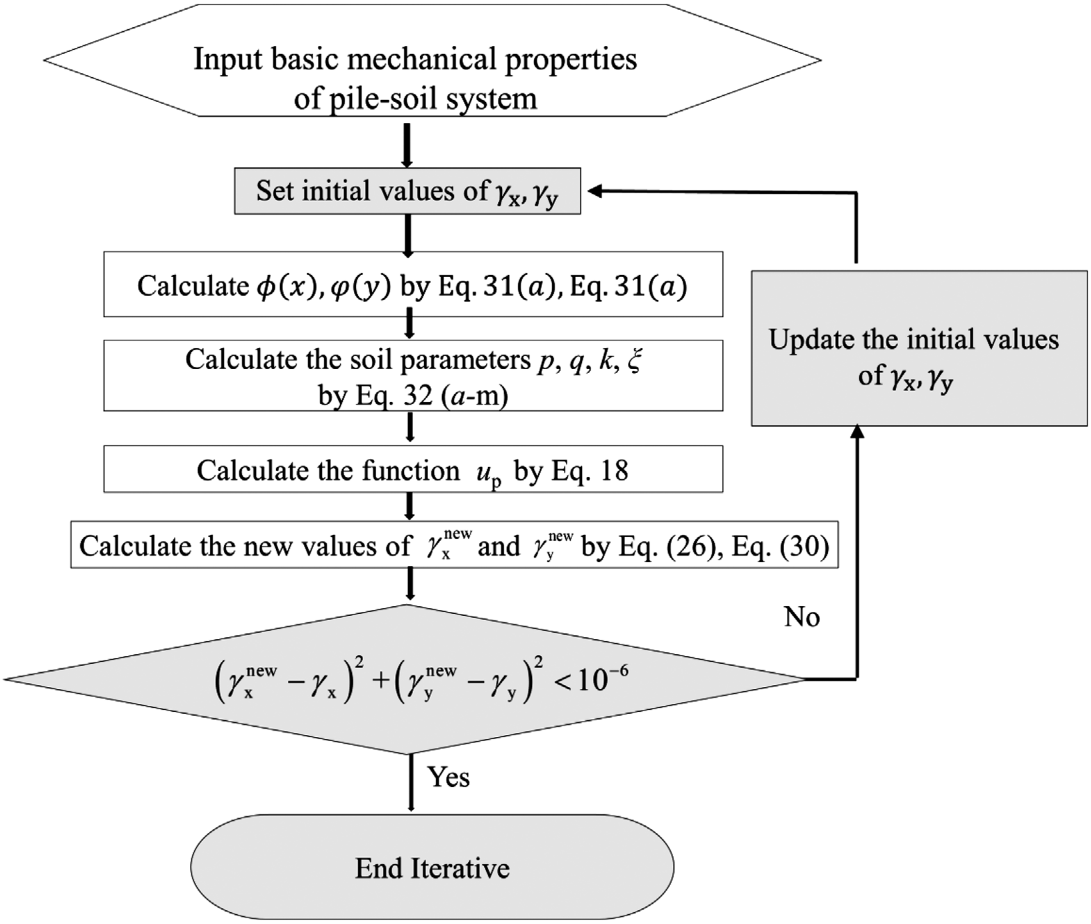

FIGURE 2 Flow chart of the iterative algorithm of MIP

$$\xi = \frac{r_p^2}{\gamma_x^2} + \frac{4a^2}{\gamma_x} \tag{34}$$

$$k = 2G_s^* (1 + 2\gamma_x) \tag{35}$$

3.4 | Modulus modification and solution algorithm

Neglecting the horizontal displacement of soil domain brings an artificial restraint and make the pile-soil system slightly stiffer. The study by Seo et al.[37] shows that the influence of this restraint could be reduced by treating the coefficient λ_s in the matrix of Equation (8) as zero and replacing the coefficient G_s^* with $0.6G_s^*(1 + 1.25{\upsilon_s}^2)$. This replacement approximately accounts for the influence of the horizontal displacement of the soil medium by modifying the coefficient in stress-strain relationship in the vertical direction. Similar modulus modification for circular piles was made in Anoyatis and Mylonakis[17] and Gupta and Basu.[23]

There are only two dependent unknown parameters γ_x,γ_y to obtain the dynamic pile impedance and soil attenuation factor. However, their explicit expressions are entangled with serval nonlinear formulas of soil parameters k, ξ, and decay functions $\phi(x)$,$\varphi(y)$. Here a conventical method of initial parameters (**MIP**, referred[43–45]) is used to find the proper values of the necessary parameters γ_x,γ_y with the aid of iterative technique. Figure 2 shows the flowchart for the iterative process of MIP. The empirical initial values of γ_x,γ_y are around 1.0. A MATLAB script is developed to obtain the solutions. The satisfactory results for the given cases in this study can converge within less than 100 steps of iteration, and the computational time is less than 10 s in a desktop with Intel core i7-9700 @3.00 GHz and 16 GB RAM.

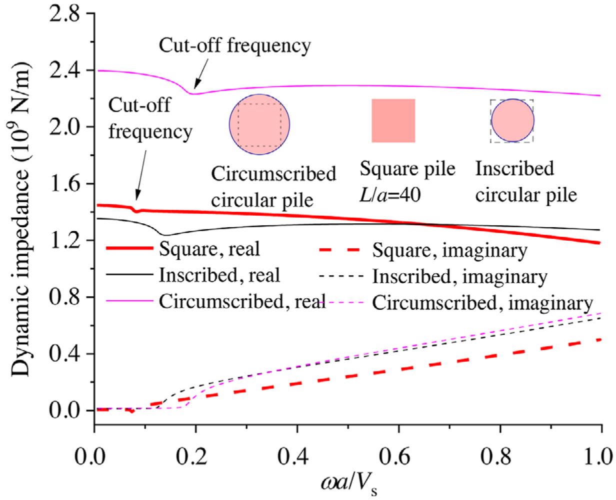

FIGURE 3 Comparison of dynamic pile impedance between square and circular piles ($L/a = 40$, $E_p/E_s = 1000$, $\beta_0 = 0.02$, $\upsilon_s = 0.4$, $\rho_p/\rho_s = 1.136$)

4 | RESULTS ANALYSIS BASED ON ANALYTICAL SOLUTIONS FOR SINGLE SQUARE PILES

4.1 | Comparison with circular piles

Gupta and Basu[23] proposed an energy-based solution for the dynamic responses of a circular pile, which was proved to be of considerable accuracy compared with the ridiculous solution by Zheng et al.[18] Here we analyze the effects of cross-section using that published formula and the presented solution in this study.

4.1.1 | Dynamic impedance at pile head

Figure 3 shows the comparison of a square pile and circular piles – circumscribed and inscribed – in the forms of complex dynamic impedance at pile tops. Note that the diameter (2r) of the two used circular piles is equal to the side length (2a) and diagonal length of the square cross section, respectively. The circular frequency$\omega$is nondimensionalized by the formula$a_0 = \omega a/V_s$, in which a_0 is a dimensionless frequency and V_s is the shear wave velocity of soil. It is observed that frequency-dependent variation trends of both real and imaginary parts of the two circular piles, though the values of cut-off frequency are different. In addition, the real part of the square pile is less visible than that of its inscribed circular pile and quantitatively close to those of circumscribed circular pile. The stiffness decrease and energy loss increase around the cut-off frequency is less significant for square piles than the circular piles, which make the variation of dynamic impedance with frequency is smoother in the square pile.

4.1.2 | Soil attenuation factor

The wave propagation in soil is also a critical physical quantity in the problem of pile-soil dynamic interaction. Figure 4 shows the variation of soil attenuation factor (calculated by u_s/u_p, a complex number that generally ranges from -1 to 1) with respect to the frequency for square and circular piles. Note that the side length direction ($\theta = 90°$) and diagonal direction ($\theta = 45°$) are selected to analyze the soil attenuation factor for square cross section. It can be seen that the soil attenuation factors strongly fluctuate with increasing frequency. Generally, the larger the distance from the concerned soil position to pile axis is, the more intensive the fluctuation of soil attenuation with frequency. Figure 4A shows that, at $s = 2a$, the real part of soil attenuation factor in a square pile is usually larger than those of corresponding inscribed circular pile at relatively low dimensionless frequency range ($0 < a_0 < 0.5$). As a_0 increases to a value around 4, that trend tends to be opposite. The frequencies dividing the monotone interval of the imaginary part of soil attenuation curve differ from

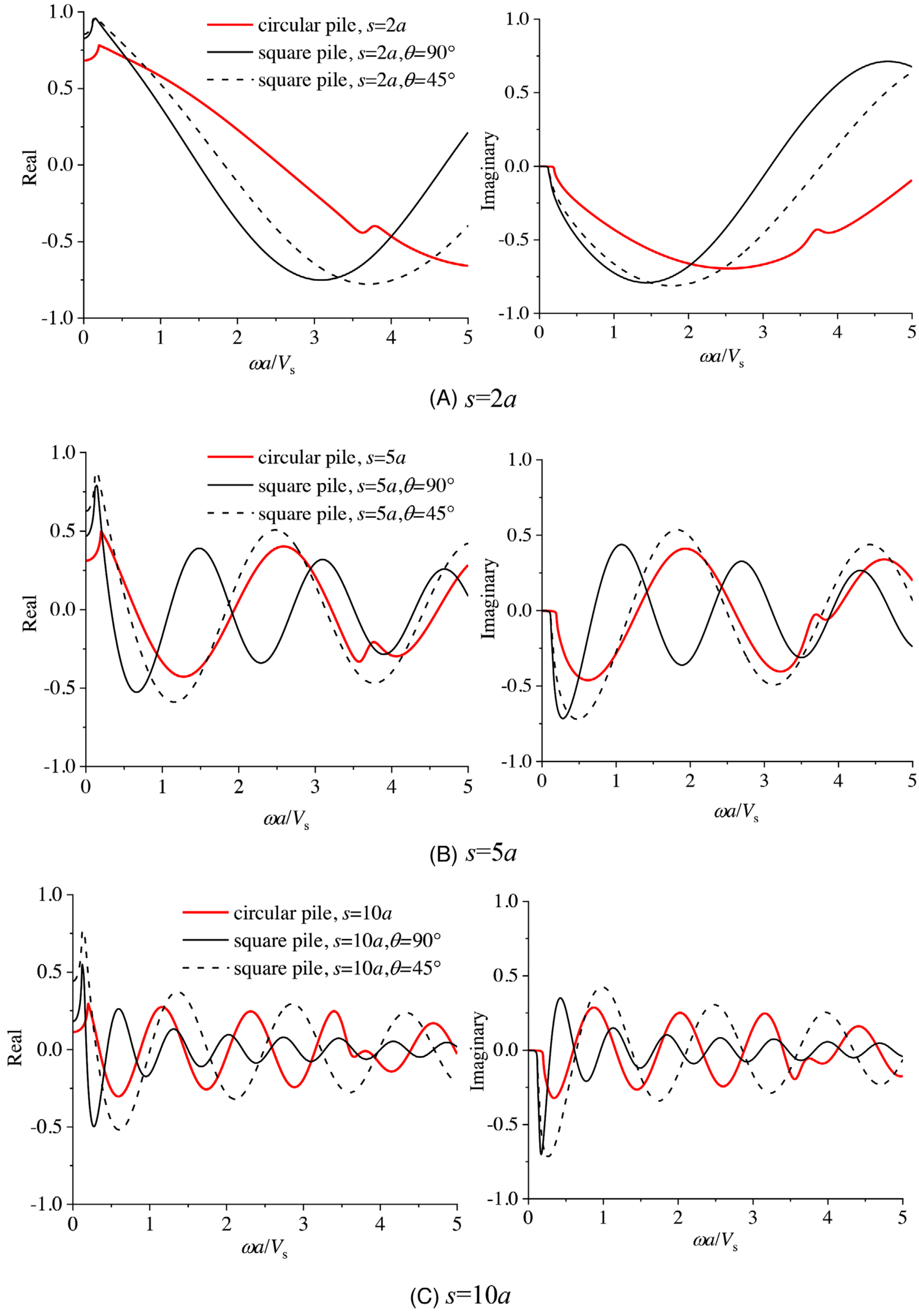

FIGURE 4 Comparison of soil attenuation factors between square and circular piles, $E_p/E_s = 1000$, $\rho_s/\rho_p = 0.88$, $L/r_p = 25$, $\mu = 0.4$

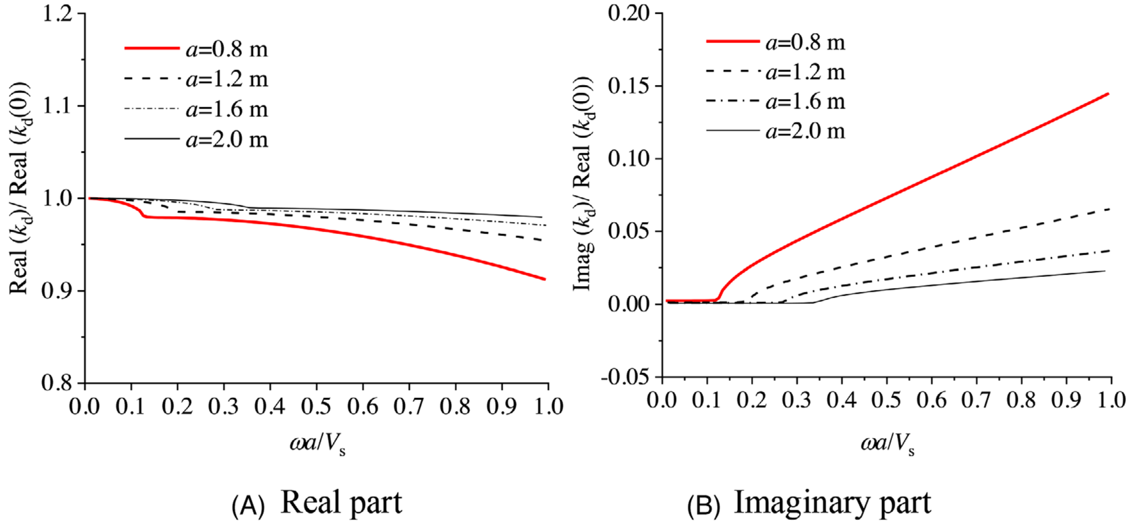

FIGURE 5 Variation of dynamic axial impedance at pile head with various side length

that of the real part. Figure 4B and C shows that the first amplitudes on frequency curves of the soil attenuation factors for the inscribed circular pile are generally smaller than that for the square pile, along both the side length direction and diagonal direction. As the frequency increases, the amplitudes of soil attenuation factors for the inscribed circular pile tend to fluctuate between the side length direction and diagonal direction for the square pile. Besides that, the cross-section effects are evidenced by the significant differences observed between the different directions, say $\theta = 90°$ and $\theta = 45°$. Figure 4A–C also reveals that the waves in soil attenuate faster along the diagonal direction in a square pile.

4.2 | Parameter analysis

In this section, case studies are carried out to analyze the roles of main geometrical and mechanical parameters on the dynamic impedance and soil attenuation. Otherwise specified, the following mechanical parameters of pile and soil are used: $\rho_s = 2500$ kg/m3 and $\rho_s = 2200$ kg/m3, $E_s = 25$ MPa, $E_p = 25$ GPa; $a = 0.8$ m, $L = 20$ m,$\upsilon_s = 0.4$, β_0=0.02.

4.2.1 | Influences of side length and soil modulus on the dynamic impedance at a pile top

Figures 5 and 6 show the influences of side length and soil modulus on the dynamic vertical impedance at the head of a pile, respectively. Note that the dynamic impedance has been normalized with respect to corresponding static stiffness, namely real(k_d)/ real(k_d(0)). From Figure 5, it can be seen that the real part of dynamic vertical impedance increases when side length increases, whereas the increasing rate tends to decrease. On the other hand, the variation curves of the real part of dynamic impedance tend to be mild with increasing frequency. The right diagram of Figure 5 clearly shows that the imaginary parts of dynamic impedance are quite small and approximately keep zero before the cut-off frequencies. As the frequency becomes larger than the cut-off frequencies, the imaginary parts that represent the damping induced energy loss gradually increases with frequency. Furthermore, the piles of larger side length generally produce weaker imaginary parts, which accounts for the aforementioned milder variation with frequency. Also note that the value of cut-off frequency increases with increasing side length, which agrees with the results that the cut-off frequency is opposite to the slender ratio L/r for circular piles by Anoyatis and Mylonakis.[17]

Figure 6 shows that the cut-off frequencies of both the real and imaginary parts of dynamic impedance are apparently affected by the modulus variation. The left diagram in Figure 6 reveals that the real parts evidently decrease as the soil modulus increases. A similar trend is also reported for the end-bearing circular piles by Gupta and Basu.[23] That phenomenon is caused by a significant growth of the imaginary components, as shown in the right diagram in Figure 6; this indicates that the inertial energy loss would increase when the soil becomes stiffer and the soil damping ratio holds.

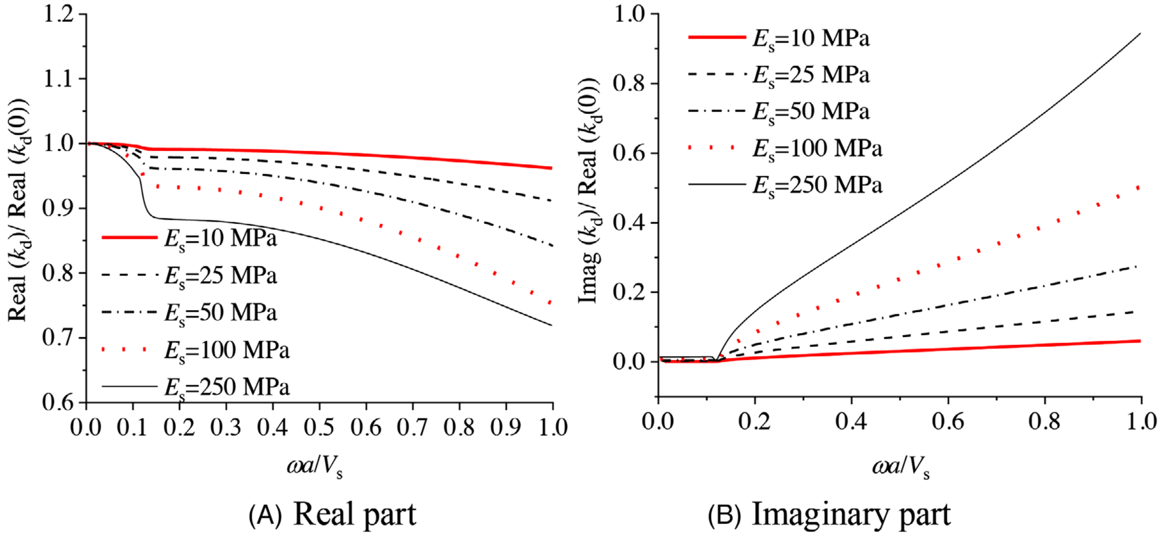

FIGURE 6 Variation of dynamic axial impedance at pile head with various soil modulus

4.2.2 | Influences of side length and soil modulus on soil attenuation factor

A common frequency range $0 < a_0 < 0.5$ is adopted for the following analysis. Figure 7A depicts the influences of the pile length on the soil attenuation factors along the directions $\theta = 45°$ and $\theta = 90°$ around a square cross section at $s = 2a$. It is observed that the real parts of soil attenuation factor increase with the frequency and has a maximum before $a_0 = 0.3$, then start to decline with a relatively stable rate. The longer the pile shaft is, the frequency at the maximum soil attenuation factor becomes smaller, which is dominated by the variation of imaginary parts shown in the right diagram in Figure 7A.

Besides that, the differences of soil attenuation factor along the directions $\theta = 45°$ and $\theta = 90°$ tend to evidently decrease as the real parts approach the maximum value. Also note that an increasing pile length would make the frequency-dependent fluctuation of soil attenuation factors become mild. Consequently, the cross-section effects would be impaired or suppressed in the square pile of greater slender ratio. Similar results can be found in Figure 7B and C.

Figure 8 shows the influences of the soil modulus on the soil attenuation factors along the directions $\theta = 45°$ and $\theta = 90°$ around a square cross section. It is prominent that the real parts of soil attenuation factor would decrease, and the peak tends to be a plateau as soil modulus increases. The influences of soil modulus on the soil attenuation are smaller than that responsible for propagation directions. Consequently, the curves in Figure 8 appears to develop into two groups: $\theta = 45°$ and $\theta = 90°$. The differences between the two interest directions vary with the fluctuation that is affected by the frequency and the distance from the pile axis. Figure 8 also reveals that soil modulus has a small influence on the real parts when the excitation frequency exceeds the cut-off frequency. Such trend can be attributed to the little variation of the imaginary parts of the soil attenuation factor as soil modulus varies, which is shown in the right diagrams in Figure 8A–C.

5 | VALIDATION AND CORRECTION OF THE DYNAMIC PILE-SOIL-PILE INTERACTION THROUGH NUMERICAL ANALYSIS

5.1 | Method description

Section 4 has proved that the proposed analytical method can obtain the satisfactory dynamic responses for the pile shaft. **However, the accuracy of responses for surrounding soil has not been confirmed**. In this section, three-dimensional finite element (FE) simulation through Abaqus software is done to reveal the wave propagation involving dynamic pile-to-pile interaction in the form of amplitude and phase.[31,34,46] The material assumption and geometrical settings are same with that in Section 2. A harmonic excitation of 1 kN is applied on the pile top in the form of distributed load and the frequency range is set from 0.5 Hz to 10 Hz. The pile properties are: mass density ρ_p 2500 kg/m^3; Young's modulus E_p 25 GPa, Poisson's ratio 0.01, side length $2a = 0.8$ m, shaft length $H = 40$ m; soil properties are: mass density ρ_s 2200 kg/m^3, Young's modulus E_s = 25 MPa, Poisson's ratio 0.3. Figure 9 shows the finite element discretization for

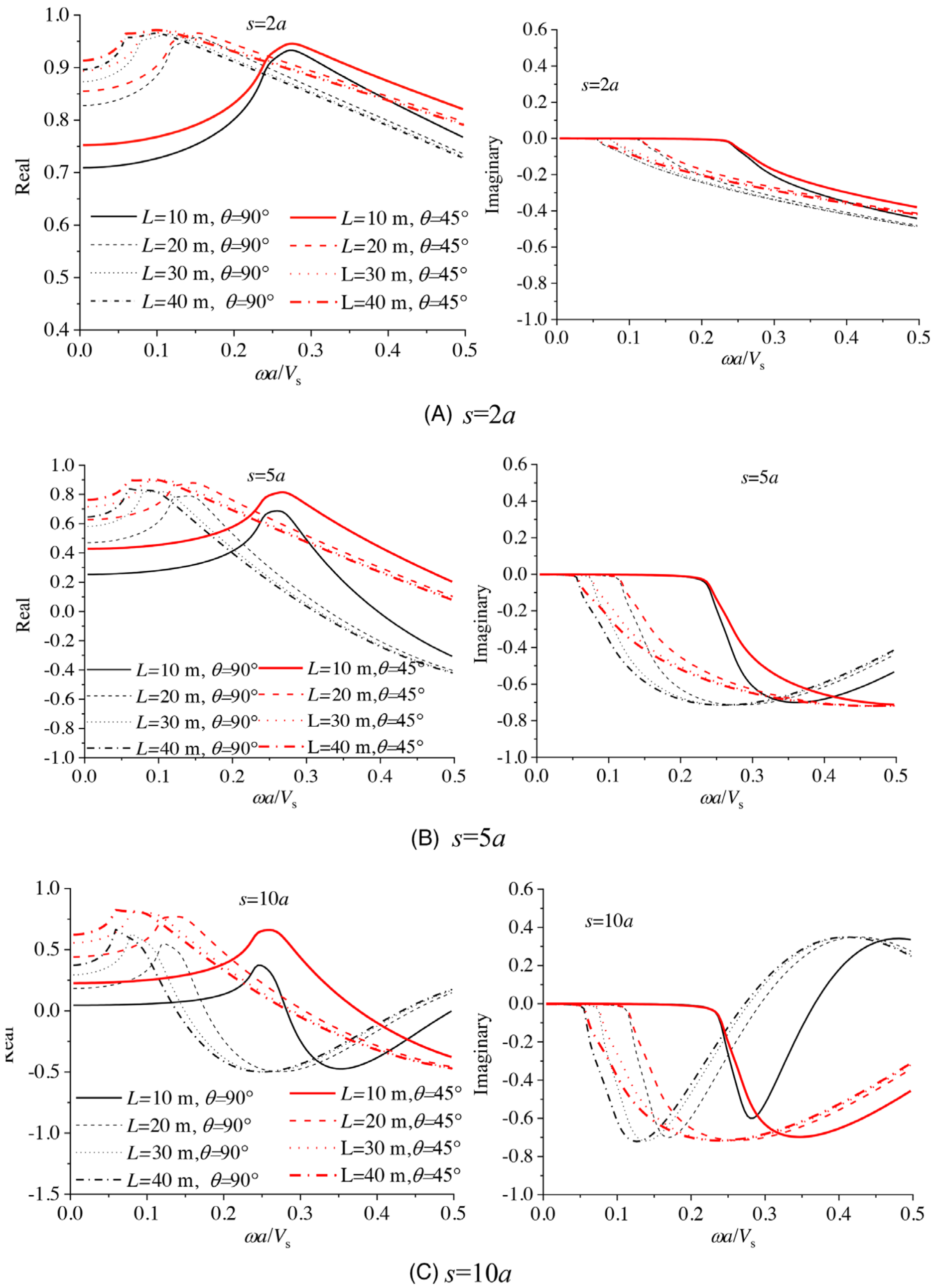

FIGURE 7 Variation of soil attenuation factor for various pile lengths ($a = 0.8$ m, $E_s = 100$ MPa, $E_p = 25$ GPa, $\rho_s = 2200$ kg/m^3, $\rho_p = 2500$ kg/m^3)

calculating pile-to-pile interaction along different wave propagation directions. Infinite element technique is employed at the lateral boundary to minimize the effects of reflected waves while the bottom boundary is fixed to simulate rigid base. A Rayleigh damping of $\kappa = 2\%$ is attributed to soil to account for material damping effects. The values of two coefficients α and β in Rayleigh damping are calculated with the first two natural frequencies ω_1 and ω_2 of pile-soil system by $\alpha = 2\kappa\omega_1\omega_2/(\omega_1 + \omega_2)$ and $\beta = 2\kappa/(\omega_1 + \omega_2)$. Associated inherent vibration modes (as shown in Figure 10) and frequencies ω_1, ω_2 can be obtained through the linear perturbation step in Abaqus.

5.2 | Vibration attenuation of surrounding soil

The vibration of surrounding soil attenuates as the radial distance from pile center increases. Figure 11A shows the time history of displacement at pile top, $4a$, $10a$ and $20a$ from pile center. It is observed that the vibration attenuation process

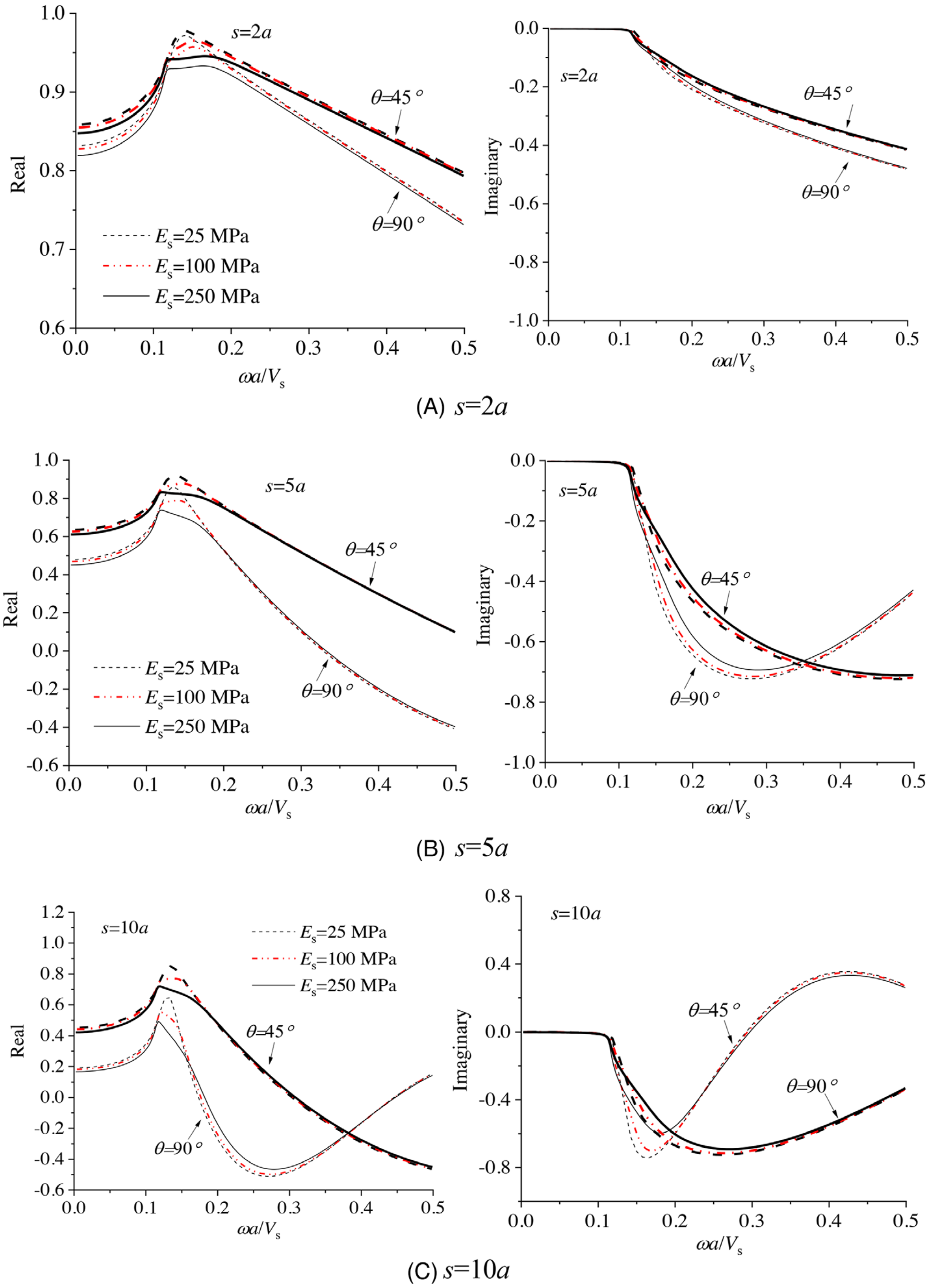

FIGURE 8 Variation of soil attenuation factor for various pile lengths ($L = 20$ m, $a = 0.8$ m, $E_p = 25$ GPa, $E_s = 25$ MPa, $\rho_s = 2200$ kg/m^3, $\rho_p = 2500$ kg/m^3)

companies with not only the amplitude decrease but also the phase lag of displacement histories. Figure 11B plots the displacement contours when the pile head comes to its lowest position around $t = 0.6$s. The vibration of pile behaves as a one-dimensional shaft and the vibration of its surrounding soil currently seems to be of axial symmetry.

Furthermore, the soil attenuation factor is calculated as the ratio of soil displacement by pile displacement at ground elevation and is expressed in the form of amplitude and phase in Figure 12. It is interesting to observe that no obvious difference for the vibration attenuation of surrounding soil along the side length direction (90°) and diagonal direction (45°).

Figure 13 shows the evolution of vertical displacement contour of pile-soil system at ground elevation. For each diagram in Figure 13, the right part plots the detailed displacement contours near the pile boundary. At the beginning of vibration

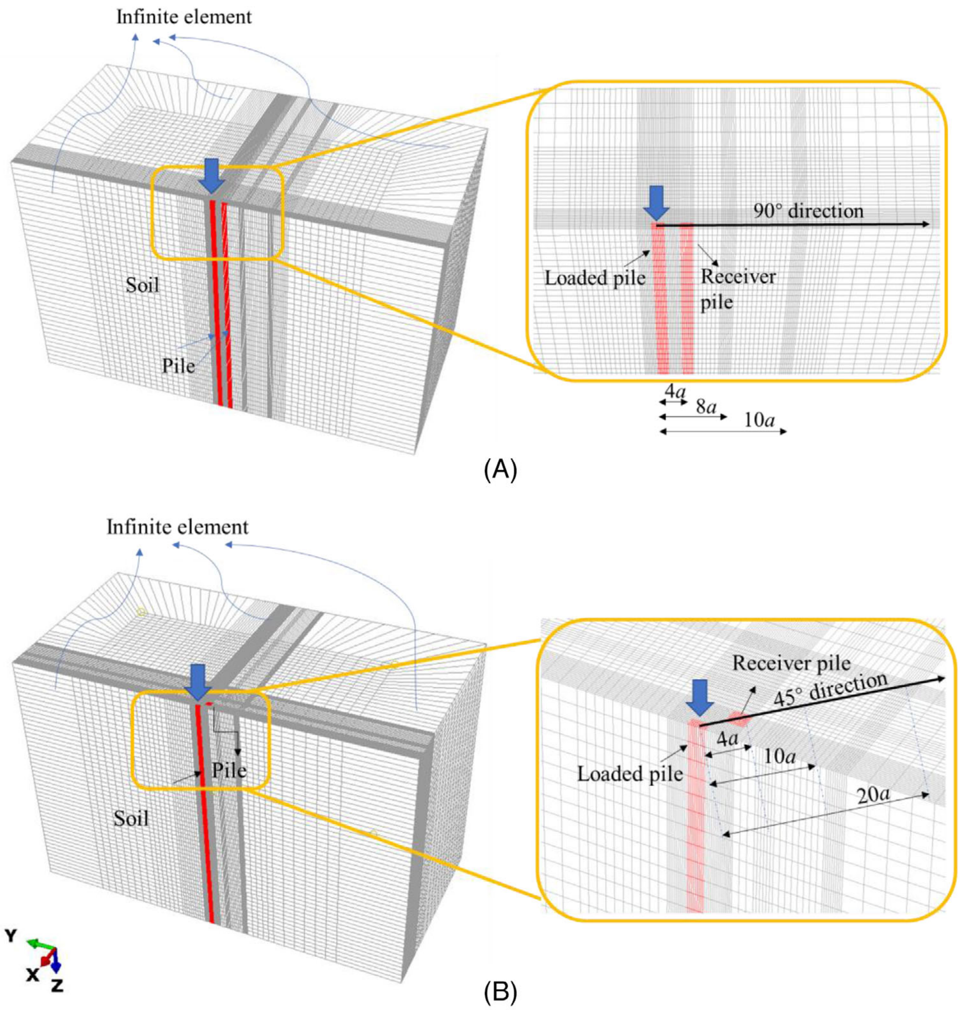

FIGURE 9 Three-dimensional finite element models: (A) model for computing the pile-pile interaction factor at $4a$ along 90° direction off the loaded pile axis; (B) model for computing the pile-pile interaction factor at $4a$ along 45° direction off the loaded pile axis

shown in Figure 13A, the displacement contours approximately close to shape of squares instead of circles, which demonstrates the effects of boundary on the soil attenuation. Very soon at $t = 0.0809$ s or around 0.011 T, the wave fronts in soil tend to become curved shape in the diagonal direction. At $t = 0.0129$ s when the wave fronts still do not arrive the radial distance of $4a$ from pile center shown in Figure 13C, it seems that the outer contours have evolved into groups of concentric circles even though the near-field soil attenuation is still dominated by the square shape contours. It reflects that the travelling waves along various directions have differential phase velocities due to the non-circular boundary. As the waves continue to propagate in Figure 13D and Figure 13E, the ratio of propagation distance to the pile dimensions gradually increases. Simultaneously, the influence of pile geometry on the soil vibration tend to be weak and thus the cylindrical waves tend to dominate the far-field soil vibration.[47] The evolution of displacement contours reflects that the square boundary plays a significant role on the surrounding soil attenuation in a range less than $4a$ off the pile axis.

Figures 14–16 show the comparisons of numerically produced soil attenuation factor with three analytical solutions: one is the classical method based on plane strain assumption by Gazetas and Makis[28]; one is the continuum-based method proposed by Basu et al.[23]; and the last is the continuum method proposed in Section 3 for square piles. Note that equivalent radius is calculated to employ the formula from circular piles by: $r_e = \sqrt{4ab/\pi}$. The results in Figure 14 show that the continuum method for square piles significantly overestimates both the amplitude and phase lag compared with Finite element (FE) numerical method. Generally, the methods for circular piles by Basu et al.,[23] Gazetas and Makis[28] can give a relatively good prediction for the soil attenuation around a square pile, especially for the frequencies larger than 1 Hz. In addition, it is also found that the amplitude from Gazetas and Makis[28] has greater deviation than that from Basu et al.,[23] which is because that the vertical wave propagation and material damping in soil is neglected in Gazetas and Makis'

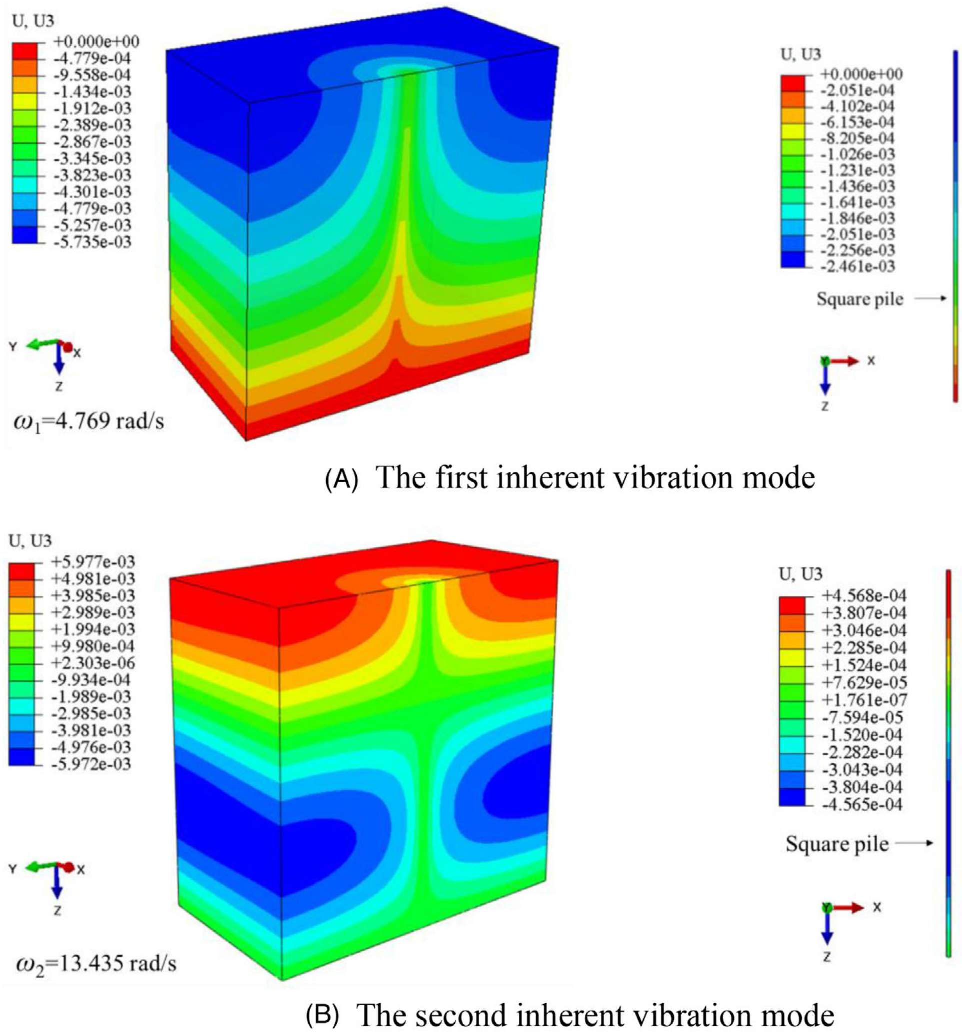

FIGURE 10 The first two vertical vibration modes of soil-pile system for computing Rayleigh damping coefficients. The unit for the displacement (U) is mm

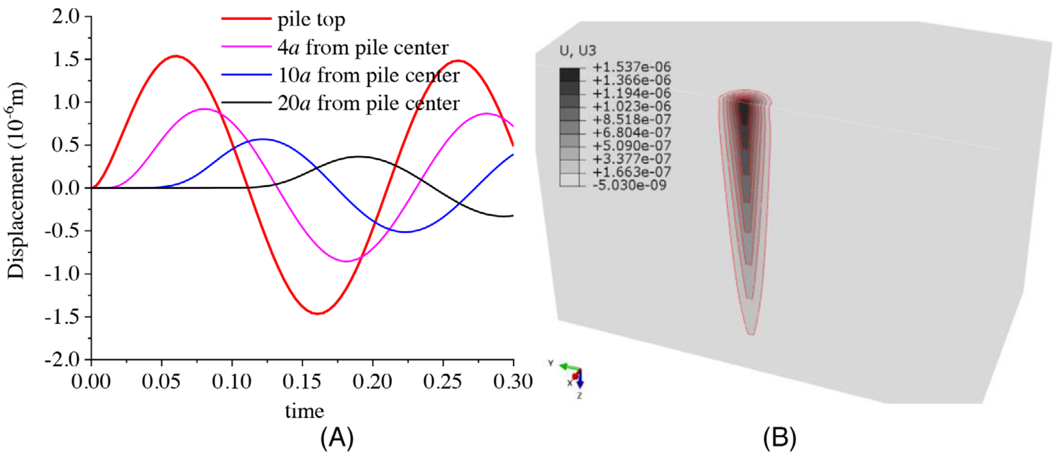

FIGURE 11 Time histories and displacement contour of pile-soil system on harmonic vibration: (A) Time histories of the vertical displacement at pile top and the interest soil positions at ground that have various radial distances from pile center; (B) displacement contour of pile-soil system when the pile displacement gets its positive peak. The unit for the displacement (U) is mm

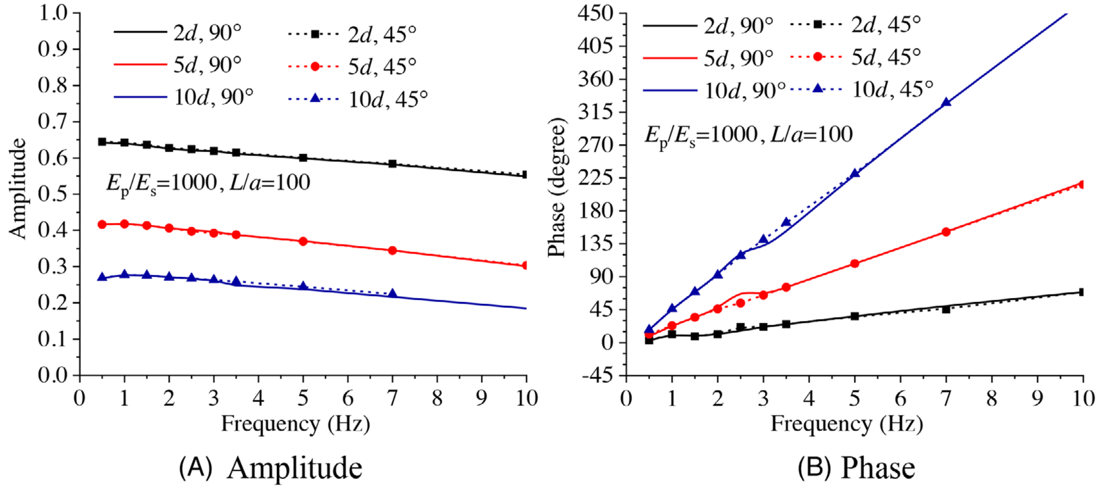

FIGURE 12 Soil attenuation factor along different directions (90° and 45°)

method. As the radial distance from pile center increases to 10a and 20a, the continuum method for square piles gives worse estimation for soil attenuation factor as observed in Figures 15 and 16. At the same time, the continuum method for circular piles from Basu et al.[23] remains to produce satisfactory soil attenuation factor, which also demonstrates that the square pile boundary exerts a weak influence on the far-field vibration of surrounding soil. Actually, it was also found that the soil attenuation characteristics around a non-circular (barrette) pile was similar to that around a circular pile in finite element analysis for the static problem.[37]

Why the continuum method for square piles yields so prominent error? Based on the displacement model for single square piles in Section 2.1, the mathematical soil attenuation functions at the area of $y > 0$ (shown in Figure 17A) can be written as following expressions:

$$\psi(x,y) = \phi(x)\varphi(y) = \begin{cases} e^{\left(-\frac{\gamma_x}{r_p}(x-a)\right)}, (x,y) \in D_1 \\ e^{\left(-\frac{\gamma_y}{r_p}(y-b)\right)} e^{\left(-\frac{\gamma_x}{r_p}(x-a)\right)}, (x,y) \in D_2 \\ e^{\left(-\frac{\gamma_y}{r_p}(y-b)\right)}, (x,y) \in D_3 \text{or} (x,y) \in D_4 \\ e^{\left(-\frac{\gamma_y}{r_p}(y-b)\right)} e^{\left(\frac{\gamma_x}{r_p}(x+a)\right)}, (x,y) \in D_5 \\ e^{\left(\frac{\gamma_x}{r_p}(x+a)\right)}, (x,y) \in D_6 \end{cases} \tag{31}$$

From Equation (31), the soil attenuation in D_1 and D_6 is independent with y coordinate, thus the displacement contour in D_1 and D_6 should be lines parallel to y axis. Similarly, the soil attenuation in D_3 and D_4 is independent with x coordinate, thus the displacement contour in D_3 and D_4 should be lines parallel to x axis. When the pile has a square cross section, $\psi(x,y)$should be symmetric with respect to $y = x$ in D_2 and be symmetric with respect to $y = -x$ in D_5. Consequently, based on the displacement model in Section 2.1, the soil displacement contours around a square pile can be illustrated as Figure 17B. The contours in Figure 17B are somewhat like that in Figure 13A, which reflects that the displacement model in Section 2.1 can explain the pile-soil interaction in the near field. However, as the radial distance from pile center increases, that displacement model causes growing error for the vibration response of far-field soil ($s > 4a$). In Figure 17C, a modified displacement model is proposed to distinguish the variation of soil attenuation pattern in the near-field and far-field.

5.3 | Dynamic interaction between piles

Figure 18 shows the dynamic interaction factors of square piles in forms of amplitude and phase from the numerical analysis. It's interesting to observe that the amplitude of passive piles at 90°direction is slightly larger than that at 45°direction

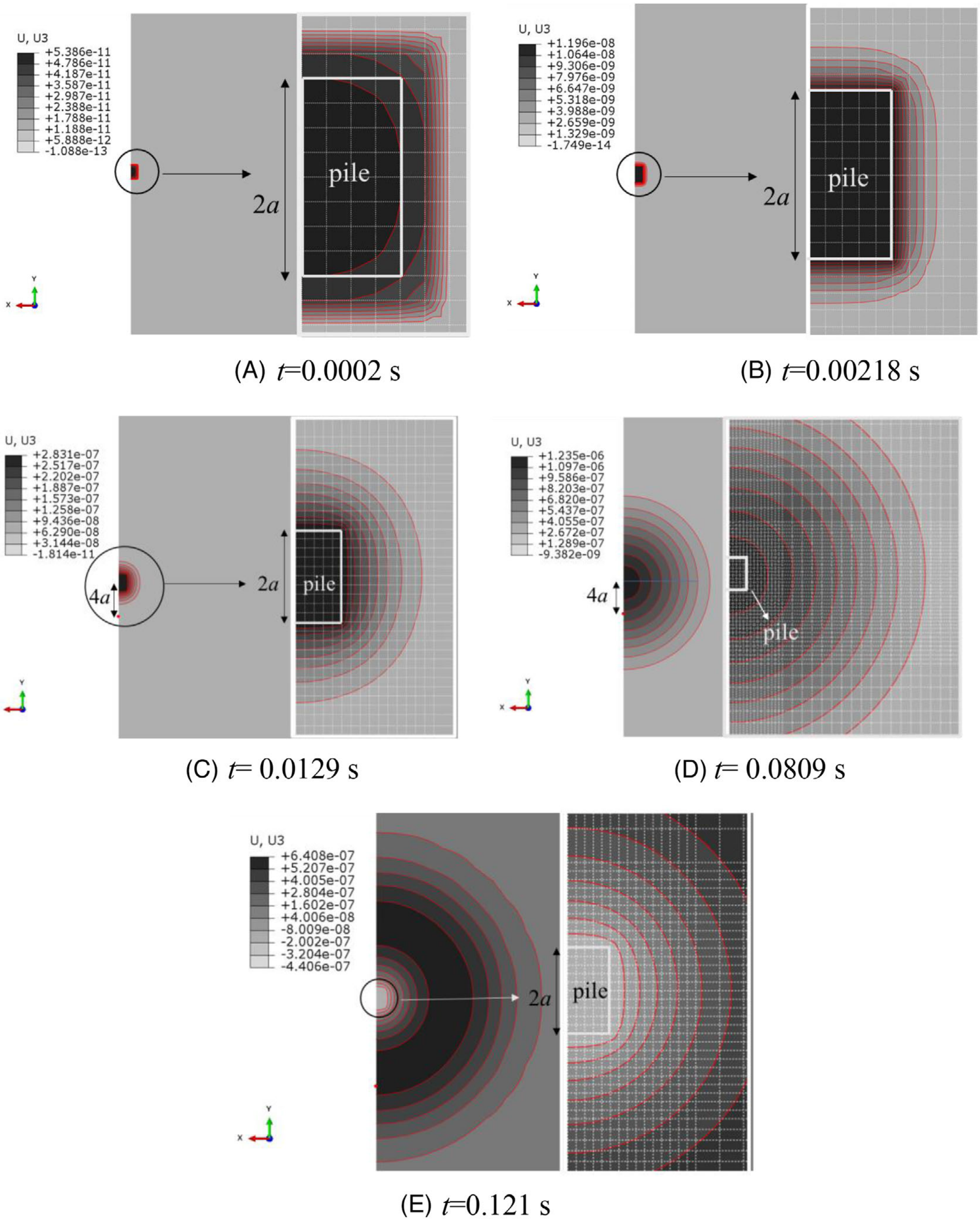

FIGURE 13 Vertical displacement contour maps of pile-soil system at ground for various time ticks. The unit for the displacement (U) is mm

at low frequency range (say less than 3 Hz). That difference tends to decrease as the excitation frequency grows. Moreover, the direction dependent difference continuously falls as the radial distance s off loaded pile increases from $4a$ to $20a$. In other words, the difference of interaction factors along 90° and 45° is generally not significant, specifically for a relatively scattered arrangement of pile group on a harmonic excitation with frequency greater than 3 Hz. In contrast, the phases of striking waves from different directions do not indicate obvious deviation, which demonstrates that the vibration waves approximately arrive to the passive piles located various direction at the same time.

For the sake of convivence, the variation of pile-to-pile interaction factor along different paths is neglected in hereafter analytical study. Consequently, the soil attenuation factor ψcould be approximated by the existing method for the soil vibration around a circular pile,[23] which has been proved to be efficient in Section 5.2. Based on the governing equation for a square pile in Section 2.2 (Equation (18)), the dynamic soil resistance k_s that acting on a square pile shaft has the

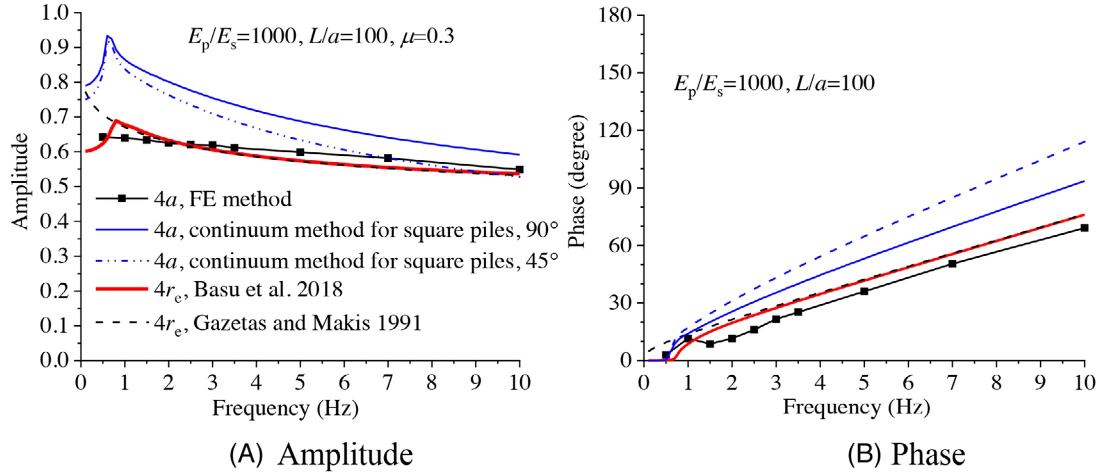

FIGURE 14 Comparisons of numerically produced soil attenuation factor with analytical solutions: radial distance 4a

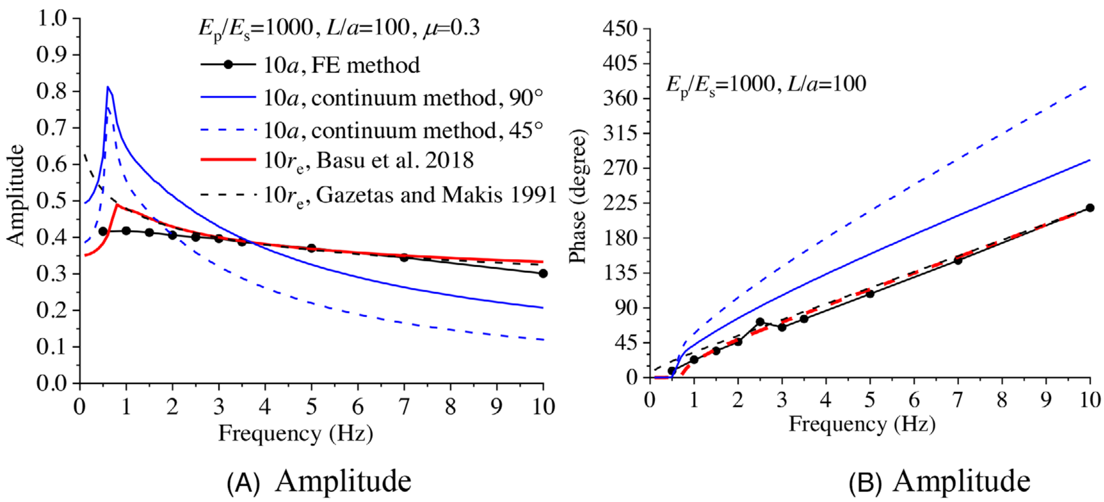

FIGURE 15 Comparisons of numerically produced soil attenuation factor with analytical solutions: radial distance 10a

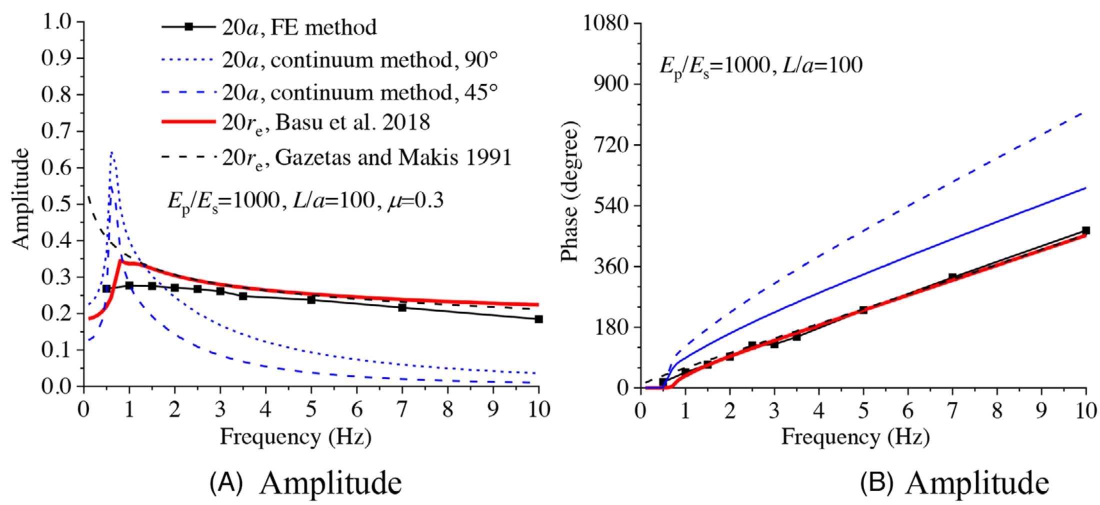

FIGURE 16 Comparisons of numerically produced soil attenuation factor with analytical solutions: radial distance 20a

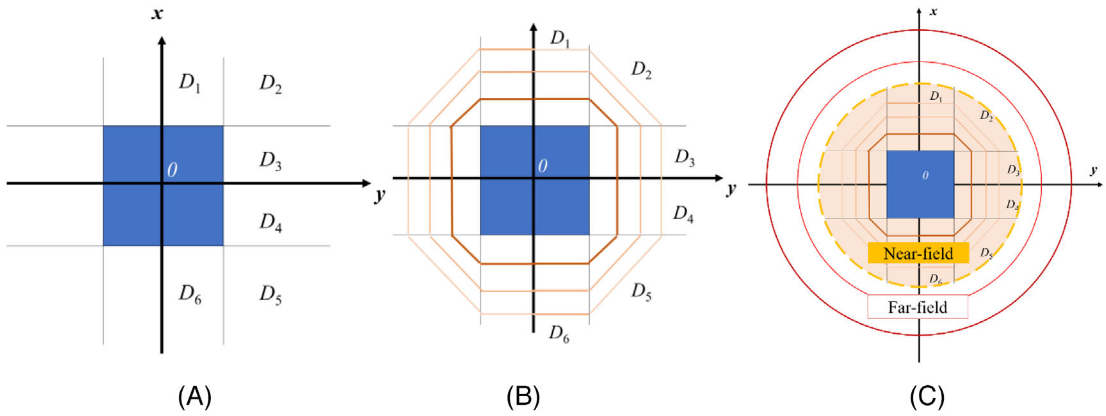

FIGURE 17 Illustration of displacement contours for square piles. (A) Partitions of soil field when $y > 0$; (B) Displacement contour illustration on the continuum theory; (C) Modified displacement contour illustration based on the FE numerical results

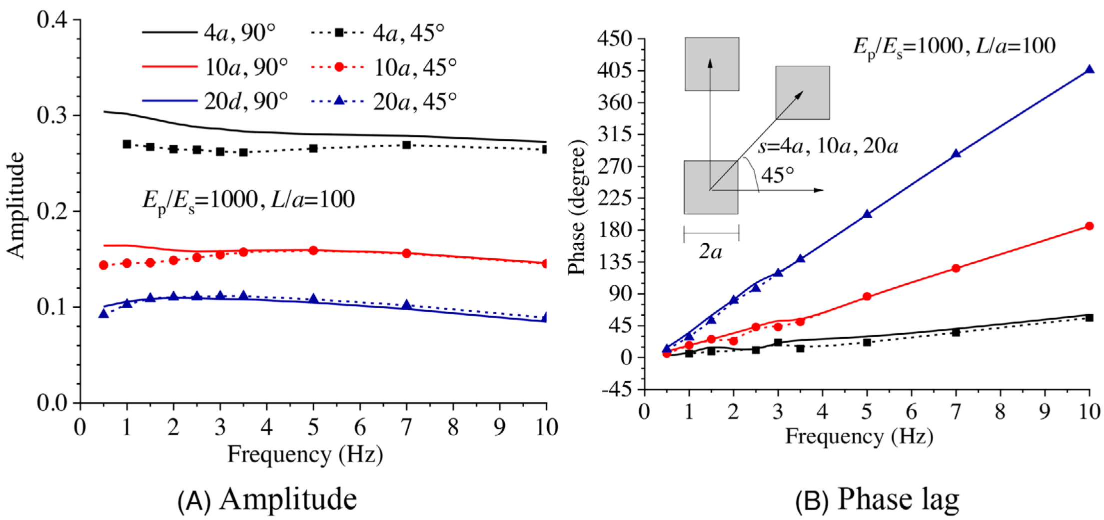

FIGURE 18 Pile to pile interaction factors of square piles along different directions

following expression:

$$k_s = k - \omega^2 \rho_s \xi \tag{32}$$

where k can be calculated through Equation (19). Diffraction factor ξ can be obtained by introducing Equation (32) into Equation (4). Then, the formula in Section 2.2 (Equation (3)) is used to calculate the interaction factors αbetween square piles. That solution to interaction factors based on the approximate soil attenuation factor is called "approximate method". Instead, if the interaction factors are calculated based on the displacement decay functions from continuum model in Section 2.1 (or 4.1.2), it is called "continuum method".

Figures 19–21 show the amplitude and phase of interaction factors from different methods. The results in Figure 19 show that the presented approximate method slightly underestimates the amplitude but does not cause obvious phase deviation at $s = 4a$. That mild underestimation is due to the one-dimensional assumption for the passive piles, which had been elaborated by Luan et al.[48] As the radial distance increases, the difference between the approximate method and FE numerical method gradually decreases as shown in Figures 20 and 21. For a comparison, the interaction factors using the soil attenuation factor based on the continuum method for square piles are also calculated. It is observed that prominent error occurs through the continuum method for both the amplitude and phase, especially when $s = 10a$ and $20a$. Considering that the effects of square boundary on the dynamic interaction factor is not significant, the proposed approximate method could give a satisfactory estimation for the pile-pile interaction factor.

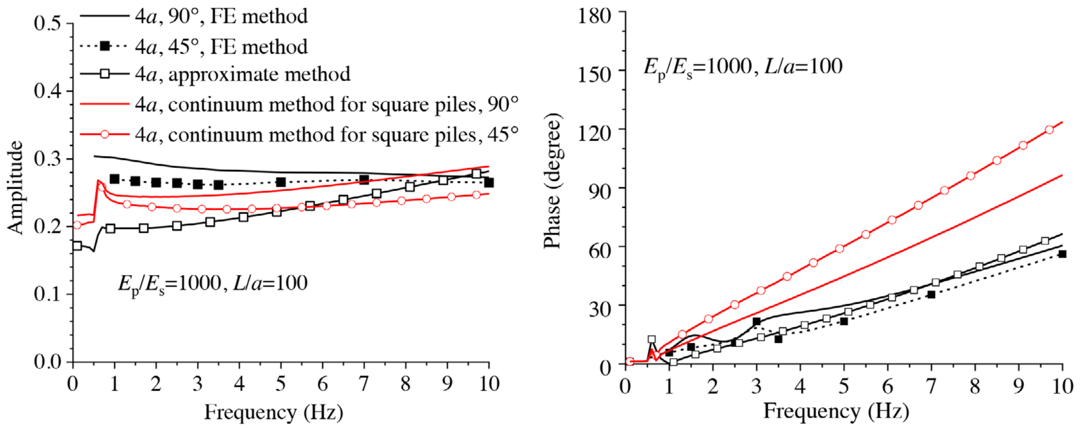

FIGURE 19 Comparisons of numerically produced interaction factor with analytical solutions: radial distance 10*a*

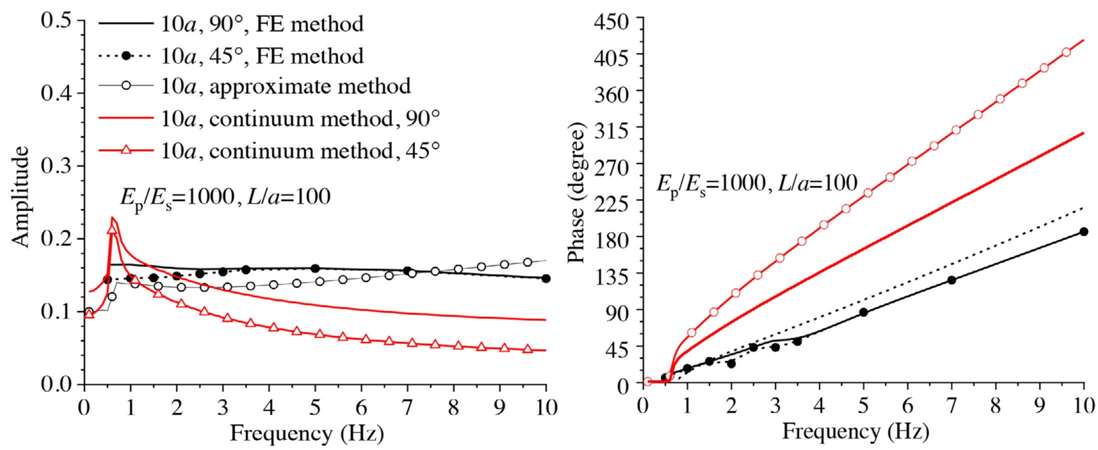

FIGURE 20 Comparisons of numerically produced interaction factor with analytical solutions: radial distance 10*a*

6 | DYNAMIC IMPEDANCE FOR GROUP OF SQUARE PILES

To now, both the dynamic impedance of a single square pile and the pile-to-pile interaction factor have been determined. Therefore, the dynamic impedance for group of square piles can be computed using the superposition principle through Equations (6) and (7). Figure 22 compares the normalized dynamic impedance for 2×2 group of square piles with that

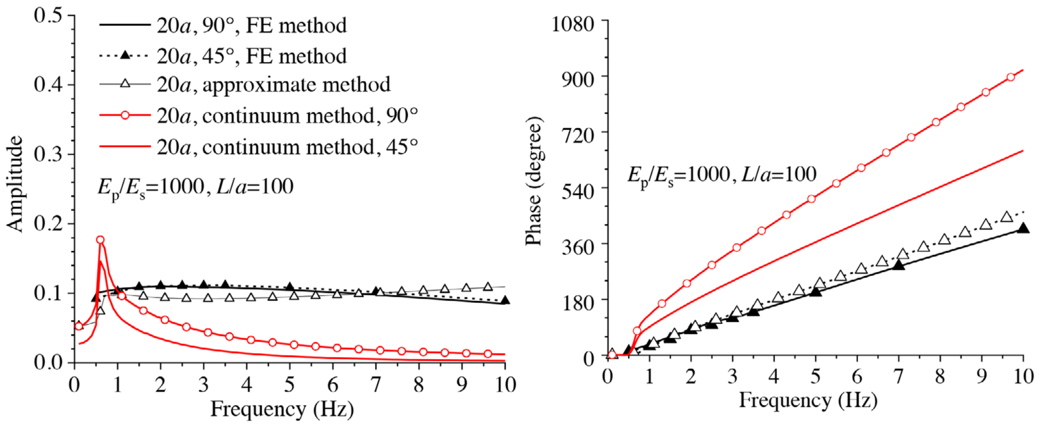

FIGURE 21 Comparisons of numerically produced interaction factor with analytical solutions: radial distance 20*a*

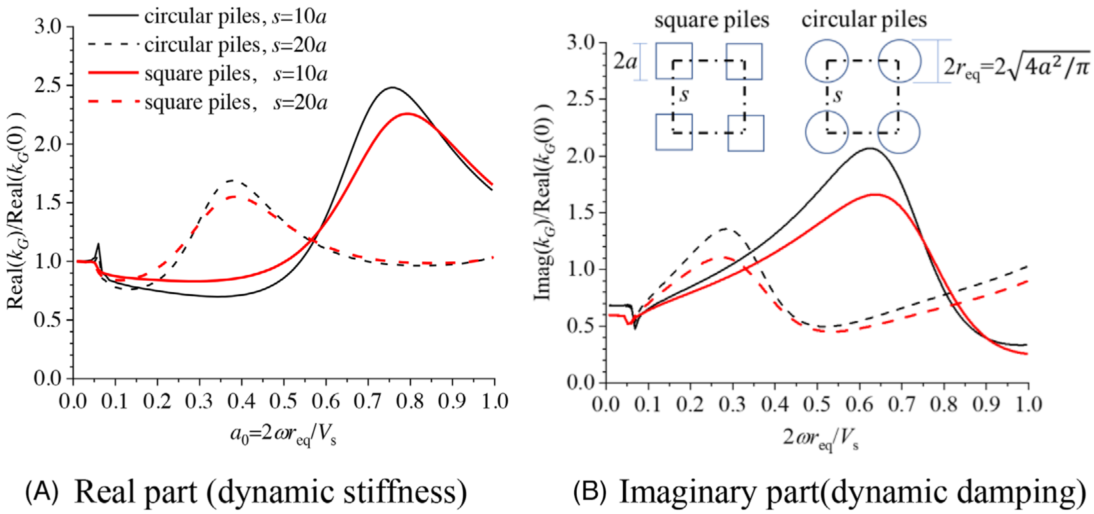

FIGURE 22 Comparison between normalized dynamic impedance for 2×2 group of square piles and circular piles. $L/a = 40$, $E_p/E_s = 1000$, $\beta_0 = 0.02$, $\upsilon_s = 0.3$, $\rho_p/\rho_s = 1.136$

for group of circular piles. The two types of groups have identical cross section area and share the same pile spacing. The results show that both the dynamic stiffness and dynamic damping in a group of square piles have smaller fluctuation against frequency. Specifically, at pile spacing $s = 10a$, the real component of dynamic impedance of square pile group is greater than that of circular pile group when the normalized frequency a_0 is less than 0.55. That positive deviation varies with frequency and is approximate to 20% at $a_0 = 0.40$. As a_0 continues to grow and exceeds 0.55, the real component of dynamic impedance of square pile group becomes smaller than that of circular pile group before $a_0 = 0.85$. That negative deviation approximately varies from 0–10% and gets its maximum around $a_0 = 0.75$. At pile spacing $s = 20a$, the fluctuation of real part of dynamic impedance is much weaker than that at $s = 10a$. At the same time, the imaginary part fluctuates more intensively due to the greater radiation damping in soil field. The impedance deviation for two types of pile groups is most obvious at around $a_0 = 0.15$ and $a_0 = 0.37$ and corresponding differences are around 12% and 8%, respectively. Those results in Figure 22 reflects that the difference of dynamic impedance between the two types of pile group could decreases with increasing pile spacing and frequency.

7 | CONCLUSIONS AND DISCUSSION

Boundary effects of pile cross section on the vibration behavior of pile-soil system are examined in this paper. The dynamic impedance of single square pile is solved by the energy-based variation principle. Complex coupling process at the pile-soil interface is avoided by introducing two individual decay functions. The effects of square boundary on the soil attenuation factor and pile-to-pile interaction factor are investigated through the combined method of numerical simulation and theoretical deduction. Based on the principle of superposition, the vertical dynamic impedance for group of square piles is obtained. For practical interest, the loading frequency is limited to a low range of $0 < a_0 < 1$ in the theoretical analysis. The following conclusions can be drawn:

1. The frequency variation of the dynamic impedance of a square pile is smoother in comparison with the circular pile. Also, a square pile generally has a less prominent stiffness decrease around the cut-off frequency than equivalent circular pile. The real parts of dynamic pile head impedance of a square pile increase with an increasing side length and decreases with increasing soil modulus. That variation is largely influenced by the imaginary parts of dynamic impedance.
2. The soil attenuation factor close to a square pile is affected by the wave propagation direction. Generally, diagonal direction attenuates slower than the side length direction and the difference is dependent on both the frequency and the distance from the pile axis. As the radial distance of interest soil positions off pile center increases, the effects of square boundary rapidly become weaker and circular pattern dominates the displacement contours of far-field soil.

3. Dynamic impedance for group of square piles generally has weaker fluctuation with frequency. The impedance deviation between those two types of pile group could decreases as pile spacing enlarges and frequency increases.

ACKNOWLEDGMENTS

This research was financially supported by China Postdoctoral Science Foundation (2021M692689); the National Natural Science Foundation Project (No: 52078426); National Key Research and Development Plan (NO. 2018YFE0207100); 2018 Sichuan province Ten thousand people plan.

AUTHOR CONTRIBUTIONS

Liming Qu: Conceptualization, Methodology, Software, Results analysis, Writing original draft. **Changwei Yang**: Software, Validation, Funding acquisition, Project administration. **Xuanming Ding**: Conceptualization, Writing review and editing, Resources, Formal analysis. **Georges Kouroussis**: Results analysis, Writing review and editing. **Cheng Yuan**: Investigation, Making scientific figures, Validation.

DATA AVAILABILITY STATEMENT

Data available on request from the authors, which means the data that support the findings of this study are available from the corresponding author upon reasonable request.

ORCID

Liming Qu https://orcid.org/0000-0002-9240-8411

REFERENCES

1. Lin SS, Liao JC. Permanent strains of piles in sand due to cyclic lateral loads. *J Geotech Geoenviron Eng*. 1999;125:798-802.
2. Tsuha C, Foray P, Jardine R, et al. Behaviour of displacement piles in sand under cyclic axial loading. *Soils Found*. 2012;52:393-410.
3. Kouroussis G, Verlinden O, Conti C. Ground propagation of vibrations from railway vehicles using a finite/infinite-element model of the soil. *Proc IME, Part F: J Rail Rapid Transit*. 2009;223(4):405-413.
4. Connolly D, Galvín P, Olivier B, Romero A, Kouroussis G. A 2.5 D time-frequency domain model for railway induced soil-building vibration due to railway defects. *Soil Dyn Earthquake Eng*. 2019;120:332-344.
5. Chen JB, Gilbert RB, Choo YS, et al. Two-dimensional lower bound analysis of offshore pile foundation systems. *Int J Numer Anal Methods Geomech*. 2015;40(9):1321-1338.
6. Choudhary SS, Biswas S, Manna B. Vertical response of 2 × 2 pile group under rotating machine induced vibrations. *Proceedings of China-Europe Conference on Geotechnical Engineering*. Springer International Publishing; 2016.
7. Chatterjee K, Choudhury D. Influence of seismic motions on behavior of piles in liquefied soils. *Int J Numer Anal Methods Geomech*. 2018;42(3):516-541.
8. Peng Y, Ding XM, Xiao Y, et al. Detailed amount of particle breakage in non-uniformly graded sands under one-dimensional compression. *Can Geotech J*. 2020;57:1239-1246.
9. Peng Y, Liu HL, Li C, et al. The detailed particle breakage around the pile in coral sand. *Acta Geotech*. 2021;16:1971-1981.
10. Li LC, Wu WB, Liu H, Lehane B. DEM analysis of the plugging effect of open-ended pile during the installation process. *Ocean Eng*. 2021;220:108375.
11. Gazetas G, Fan K, Kaynia A. Dynamic response of pile groups with different configurations. *Soil Dyn Earthquake Eng*. 1993;12:239-257.
12. Rovithis E, Mylonakis G, Pitilakis K. Dynamic stiffness and kinematic response of single piles in inhomogeneous soil. *Bull Earthquake Eng*. 2013;11:1949-1972.
13. Mylonakis G, Gazetas G. Vertical vibration and additional distress of grouped piles in layered soil. *Soils Found*. 1998;38:1-14.
14. Tian X, Hu W, Gong X. Longitudinal dynamic response of pile foundation in a nonuniform initial strain field. *KSCE J Civ Eng*. 2015;19:1656-1666.
15. Wang N, Wang KH, Wu WB. Analytical model of vertical vibrations in piles for different tip boundary conditions: parametric study and applicationsx. *J Zhejiang Univ Sci A*. 2013;14:79-93.
16. Ai ZY, Liu CL, Wang LJ, Wang LH. Vertical vibration of a partially embedded pile group in transversely isotropic soils. *Comput Geotech*. 2016;80:107-114.
17. Anoyatis G, Mylonakis G. Dynamic Winkler modulus for axially loaded piles. *Geotechnique*. 2012;62:521-536.
18. Zheng CJ, Ding XM, Li P, Fu Q. Vertical impedance of an end-bearing pile in viscoelastic soil. *Int J Numer Anal Methods Geomech*. 2015;39:676-684.
19. Militano G, Rajapakse R. Dynamic response of a pile in a multi-layered soil to transient torsional and axial loading. *Geotechnique*. 1999;49:91-109.
20. Cui CY, Meng K, Wu YJ, et al. Dynamic response of pipe pile embedded in layered visco-elastic media with radial inhomogeneity under vertical excitation. *Geomech Eng*. 2018;16(10):609-618.

21. Wu WB, El Naggar MH, Abdlrahem M, et al. New interaction model for vertical dynamic response of pipe piles considering soil plug effect. *Can Geotech J*. 2017;54(7):987-1001.
22. Cui CY, Meng K, Liang Z, et al. Effect of radial homogeneity on low-strain integrity detection of a pipe pile in a viscoelastic soil layer. *Int J Distrib Sens Netw*. 2018;14(10):155014771880645.
23. Gupta BK, Basu D. Dynamic analysis of axially loaded end-bearing pile in a homogeneous viscoelastic soil. *Soil Dyn Earthquake Eng*. 2018;111:31-40.
24. Zhang S, Cui CY, Yang G. Vertical dynamic impedance of pile groups partially embedded in multilayered transversely isotropic saturated soils. *Soil Dyn Earthquake Eng*. 2019;117:106-115.
25. Zhang YP, Liu Hao, Wu WB, et al. Interaction model for torsional dynamic response of thin-wall pipe piles embedded in both vertically and radially inhomogeneous soil. *Int J Geomech*. 2021a;21(10):04021185.
26. Zhang YP, Liu H, Wu WB, et al. A 3D analytical model for distributed low strain test and parallel seismic test of pipe piles. *Ocean Eng*. 2021b;225:108828.ID:108828.
27. Dobry R, Gazetas G. Simple method for dynamic stiffness and damping of floating pile groups. *Geotechnique*. 1988;38(4):557-574.
28. Gazetas G, Makris N. Dynamic pile-soil-pile interaction. Part I: analysis of axial vibration. *Earthquake Eng Struct Dyn*. 1991;20:115-132.
29. Wang JH, Zhou XL, Lu JF. Dynamic response of pile groups embedded in a poroelastic medium. *Soil Dyn Earthquake Eng*. 2003;23(3):53-60.
30. Luan LB, Zheng CJ, Kouretzis G, et al. Development of a three-dimensional soil model for the dynamic analysis of end-bearing pile groups subjected to vertical loads. *Int J Numer Anal Methods Geomech*. 2019;43:1784-1793.
31. Kanellopoulos K, Gazetas G. Vertical static and dynamic pile-to-pile interaction in non-linear soil. *Geotechnique*. 2020;70(2):432-447.
32. Radhima J, Kanellopoulos K, Gazetas G. Static and dynamic lateral non-linear pile–soil–pile interaction. *Geotechnique*. 2021:1-16.
33. Ding XM, Qu LM, Yang JC, Wang CL. Experimental study on the pile group-soil vibration induced by railway traffic under the inclined bedrock condition. *Acta Geotechnic*. 2020;15:3613-3620.
34. Qu LM, Ding XM, Kouroussis G, et al. Dynamic interaction of soil and end-bearing piles in sloping ground: numerical simulation and analytical solution. *Comp Geotechn*. 2021;134:103917.
35. Qu LM, Ding XM, Zheng CJ, et al. Vertical vibration characteristics of group piles in sloping topography. *Earthquake Eng Eng Vibr*. 2021;20(2):377-390.
36. Basu D, Prezzi M, Salgado R, Chakraborty T. Settlement analysis of piles with rectangular cross sections in multi-layered soils. *Comput Geotech*. 2008;35:563-575.
37. Seo H, Basu D, Prezzi M, Salgado R. Load-settlement response of rectangular and circular piles in multilayered soil. *J Geotech Geoenviron Eng*. 2009;135:420-430.
38. Zhou H, Liu HL, Kong GQ, Cao ZH. Analytical solution for stress and displacement after X-section cast-in-place pile installation. *Math Probl Eng*. 2013;2013:1-11. ID: 937421.
39. Qu LM, Ding XM, Zheng CJ, Liu HL. An analytical solution for wave propagation in a square pile due to transient point load. *Comput Geotech*. 2017;83:77-82.
40. Lv YR, Li X, Wang Y. Centrifuge and numerical modeling of geometrical effects on XCC piled rafts. *Soils Found*. 2020;60(6):1405-1421.
41. Zhou H, Liu HL, Ding XM, Kong GQ. A p-y curve model for laterally loaded XCC pile in soft clay. *Acta Geotech*. 2020;15:3229-3242.
42. Zhang C, Deng P, Ke W. Kinematic response of rectangular piles under S waves. *Comput Geotech*. 2018;102:229-237.
43. Vallabhan CVG, Mustafa G. A new model for the analysis of settlement of drilled piers. *Int J Numer Anal Methods Geomech*. 1996;20:143-152.
44. Lee KM, Xiao ZR. A new analytical model for settlement analysis of a single pile in multi-layered soil. *Soils Found*. 1999;39:131-143.
45. Qu LM, Yang CW, Ding XM, et al. A continuum-based model on axial pile-head dynamic impedance in inhomogeneous soil. *Acta Geotech*. 2021c.
46. Kouroussis G, Anastasopoulos I, Gazetas G, Verlinden O, Three-dimensional finite element modelling of dynamic pile-soil-pile interaction in time domain. *In*: *Proceedings of 4th ECCOMAS Thematic Conference*. Kos Island, Greece, 2013.
47. Gutowski TG, Dym CL. Propagation of ground vibration: a review. *J Sound Vibr*. 1976;49:179-193.
48. Luan LB, Zheng CJ, Kouretzis G, Ding XM. A new dynamic interaction factor for the analysis of pile groups subjected to vertical dynamic loads. *Acta Geotech*. 2020;15(2):3545-3558.

How to cite this article: Qu L, Yang C, Ding X, Kouroussis G, Yuan C. Vertical vibration of piles with square cross-section. *Int J Numer Anal Methods Geomech*. 2021;45:2629–2653. https://doi.org/10.1002/nag.3280